https://doi.org/10.5194/os-2019-121
Preprint. Discussion started: 3 January 2020

Ocean Science
Discussions
Open Access
EGU

Bottom-water temperature controls on biogenic silica dissolution and recycling in surficial deep-sea sediments

Shahab Varkouhi and Jonathan Wells

Department of Earth Sciences, University of Oxford, Oxford, UK

varkouhi1973@gmail.com

1 Abstract

This study calculated the dissolution rates of biogenic silica deposited on the seafloor and the silicic acid benthic flux for 22 Ocean Drilling Program sites. Simple models developed for two host sediment types—detrital and carbonate—were used to explain the variability of biogenic opal dissolution and recycling under present-day low (-0.3 to 2.14°C) bottom-water temperatures. The kinetic constants describing silicic acid release and silica saturation concentration increased systematically with increasing bottom-water temperatures. When these temperature effects were incorporated into the diagenetic models, the prediction of dissolution rates and diffusive fluxes was more robust. This demonstrates that temperature acts as a primary control that decreases the relative degree of pore-water saturation with opal while increasing the silica concentration. The correlation between the dissolution rate and benthic flux with temperature was pronounced at sites where biogenic opal is accommodated in surficial sediments mostly comprised of biogenic carbonates. This is because the dissolution of carbonates provides the alkalinity necessary for both silica dissolution and clay formation; thus strongly reducing the retarding influence of clays on opal dissolution. Conversely, the silica exchange rates were modified by presence of aluminosilicates, which led to a higher burial efficiency for opal in detrital- than in carbonate-dominated benthic layers. Though model prediction of first-order silica early transformation suggests likely effects from surface temperatures (0–4°C) on opal-CT precipitation over short geological times (< 4 Ma) near seabed in the Antarctic Site 751, the relationship between silica solubility and surface area variability in time is a more critical control. Since silica solubility

https://doi.org/10.5194/os-2019-121
Preprint. Discussion started: 3 January 2020


Ocean Science
Discussions
Open Access
EGU

and surface area decrease with time, a < 4 Ma elapsed time aged opal-A to the point that changes in specific surface area caused minor effects on solubility, allowing for formation of opal-CT at low temperature settings near the seabed.

Keywords: Bottom-water temperature, Biogenic silica, Dissolution rate, Benthic flux, Ocean Drilling Program

2 Introduction

Only a fraction of siliceous tests (~3%; Tréguer and De La Rocha, 2013) produced by plankton such as diatoms, radiolarians, and silicoflagellates in surface ocean accumulates on the seafloor after avoiding dissolution in the upper ocean and lengthy passage through the water column. Even then, this small percentage of solution resistant biogenic silica (opal-A) undergoes progressive dissolution across water-sediment interface, especially within the top few centimetres of sediment column, where 70–95% of the opal rain arriving at the seafloor dissolves prior to burial (Ragueneau et al., 2000). The extensive dissolution of siliceous tests in surface sediments—including the water-sediment interface and the first centimetres below it—constitutes part of silica early diagenesis during which a considerable volume of silicic acid produced by dissolution of opal is released back to overlying ocean water through diffusion (Dixit and Van Cappellen, 2003). This recycling (benthic flux) of silica (23×10^{12} moles of silicon per year) is estimated to be globally three times greater than the total amount of opal arriving on the seafloor and ending up buried in the sediment column (burial flux) (Tréguer et al., 1995).

Interest in the dissolution of sedimentary opal-A within deep-sea surficial sediments

https://doi.org/10.5194/os-2019-121
Preprint. Discussion started: 3 January 2020


Ocean Science
Discussions
Open Access
EGU

48 arises partly because of its importance as a mechanism by which the generated silicic acid
49 contributes as a major component of the nutrient silicon cycle in the world ocean. More
50 importantly, the part of silicic acid not diffused back to the water column and trapped in
51 pore water under burial is consumed deeper in the sediment to incite the development of
52 a diagenetic transition zone (Varkouhi, 2018)—a boundary across which biogenic silica
53 is transformed into diagenetic opal (opal-CT). This depth interval gains importance as a
54 potential energy resource (Davies and Cartwright, 2002) and as a result of the
55 significance of silica diagenesis for basin analysis approach (Wrona et al., 2017).

56 The dissolution rate of opal-A depends on a variety of factors, including temperature,
57 time, reactive surface area of biogenic opal, pore-water chemistry, host lithology, and
58 sediment permeability (Lancelot, 1973; Kastner et al., 1977; Hein et al., 1978; Nobes et
59 al., 1992; Hesse and Schacht, 2011). Among these, temperature is widely accepted as the
60 dominant control (Kastner et al., 1977; Williams and Crerar, 1985; Neagu et al., 2010).
61 The solubility of biogenic opal substantially increases with temperature (Canfield et al.,
62 2005; Atkins and de Paola, 2006; Park et al., 2006; Boggs, 2009). Laboratory based
63 experiments by Van Cappellen and Qiu (1997a) provided constraints for development of
64 mechanistic models of silica early diagenesis in marine sediments. They suggested that
65 silica solubility is dependent on bottom-water temperature for highly siliceous uppermost
66 sediments (top 10-20 cm) of the Southern Ocean, and a temperature increase of 0.5°C
67 adds up to 50 µM dissolved silica to pore water. Comparable experiments by Rickert
68 (2000), at an *in situ* temperature of 2°C to simulate bottom-water conditions, also
69 demonstrated a critical temperature dependence on dissolution of opal in the Arabian Sea.

https://doi.org/10.5194/os-2019-121
Preprint. Discussion started: 3 January 2020


Ocean Science
Discussions
Open Access
EGU

To date, the basis for most models that account for early diagenetic transport of silica through surficial sediments is derived from a first-order dissolution rate law (e.g., Schink et al., 1975; Berner, 1980; Rabouille et al., 1997; Dixit and Van Cappellen, 2003):

$$R_{diss} = k\left(1 - \frac{C}{C_{sat}}\right) \quad (1.1)$$

where R_{diss} is the dissolution rate of biogenic opal in the sediment (in s^{-1}), k is the temperature-dependent first-order kinetic constant (in s^{-1}), C is the dissolved silica concentration (in μM), and C_{sat} is the asymptotic silica concentration (in μM).

The major assumption is that the dissolution of biogenic opal supplied to the sediment through seawater opal rain produces dissolved silica. This kinetic expression of the reaction rate highlights the dependence of dissolution rate on the reaction rate constant (involving bottom-water temperature effects) and on relative departure from equilibrium with opal—given by the contrast between pore-water silica concentrations and the saturation value (the asymptotic concentration of silicic acid). The mathematical expansion of the standard kinetic rate law for opal dissolution also forms the basis of most models that deal with the benthic flux of silicic acid. Dixit and Van Cappellen (2003) presented the most comprehensive expansion of the congruent rate law for biogenic opal. Their expression for the benthic flux of silica combines the expanded dissolution rate equation (including the effects of biogenic opal content of sediment and the petrophysical properties in the magnitude of the standard kinetic rate) with Fick's first law for diffusion through a porous medium.

https://doi.org/10.5194/os-2019-121
Preprint. Discussion started: 3 January 2020


Ocean Science
Discussions
Open Access
EGU

Silica dissolution and its associated benthic flux in deep-sea sediments, as predicted by Dixit and Van Cappellen's (2003) model and the other aforementioned works, are however modified by relative detrital fraction of the sediment—implying an inverse correlation between dissolution rate and the mass ratio of lithogenic matter (detrital) to biogenic opal supply of the sediment. In opaline sediments that experience significant detrital inputs, precipitation of aluminum derived from detrital material simultaneous with dissolved silica release into the pore water slows down the dissolution rate of biogenic silica and prevents pore-water silica from reaching saturation with the dissolving opal (Van Cappellen and Qiu, 1997a; Dixit and Van Cappellen, 2003).

Despite the rate-limiting role of detrital matter in silica early diagenesis, there are indications that (bottom-water)temperatures exert a stronger control on silica dissolution and recycling that under some circumstances is even more efficient than silica pore-water concentration (Dixit et al., 2001). Evidence for a strong temperature control includes:
(1) A shift in relative saturation (from an undersaturated to a saturated state) within the detrital-dominated surficial sediments from the Ocean Drilling Program (ODP) cores (e.g., ODP Sites 794 and 795; Varkouhi, 2018) implies a strong control by bottom-water temperature on biogenic opal dissolution, even in presence of high lithogenic content.
(2) Seasonal variations of opal dissolution rate and silicic acid effluxes within the topmost sediment layer in some ocean regions (e.g., the southern North Sea) suggest a strong relationship between these processes and bottom-water temperatures. This relationship reflects low silicic acid fluxes in winter and markedly high fluxes in summer (Oehler, 2014). The increased silicic acid fluxes during summer might be inconsistent

https://doi.org/10.5194/os-2019-121
Preprint. Discussion started: 3 January 2020


Ocean Science
Discussions
Open Access
EGU

with diatoms primary production as phytoplankton blooms during summer lead to silicic acid depletion in the water column. However, silica concentration can further increase after phytoplankton blooms by settling and dissolution of diatoms at the seafloor and within the surface sediment (Joint and Pomroy, 1993);

(3) It is evident that the accumulation of ancient early diagenetic opal through time was responsive to temperature following a shift in marine silica cycle to a diatom-dominated pattern in the Late Jurassic and Cretaceous (Hein and Parrish, 1987; Kidder and Erwin, 2001; Muttoni and Kent, 2007). This shift argues that pre-Cretaceous oceans had higher levels of dissolved silica than younger basins (Siever, 1992). Effects of temperature, however, receive less focus because of limited variability in modern systems.

The main objective of this paper is to research the role of bottom-water temperature in silica dissolution and recycling across surficial layer (topmost few tens of centimetres) of marine sediment record. Here, we examine accessible ODP sources to compile and analyse data regarding lithology, temperature, silica concentrations of pore water, and physical properties of the surface biosiliceous sediments cored by the ODP. Neagu et al. (2011) reported about 100 ODP wells around the globe that drill the sediment units containing a silica diagenesis transition zone. Among these, we chose 22 sites where the transition is located in Neogene deposits for which there are existing data of the topmost sediment composition, bottom-water temperatures, pore-water silica levels, sediment porosity, and density. These Neogene transitions are developed largely free from any significant interaction with downslope processes and are identifiable through seismic and downhole profiles easier and with more certainty than those within the older successions.

https://doi.org/10.5194/os-2019-121
Preprint. Discussion started: 3 January 2020


Ocean Science
Discussions
Open Access
EGU

134 The dissolution rates of reactive silica across the surface sediment were calculated for all
135 the 22 sites using the first-order rate law, the diffusive effluxes using the early diagenetic
136 model expression of Dixit and Van Cappellen (2003), and the burial fluxes of opal using
137 the mass accumulation rate expression (Oehler, 2014). Diagenetic models accounting for
138 temperature dependence of the kinetic rate coefficient (k) were formulated to predict the
139 silica dissolution and its benthic flux in relation to modern bottom-water temperatures.
140 These results were then used to predict the transformation of biogenic opal and discuss
141 unusual precipitation of low temperature (commonly from 0 to 4 °C) young (< 4 Ma; e.g.,
142 Botz and Bohrmann, 1991) opal-CT at some Antarctic sub-seabottom locations.

143 **3 Environmental setting**

144 The distribution of 22 ODP sites studied here is indicated on Figure 1. Half of the sites
145 were drilled off the western continental margins of North and South America and within
146 the northern Pacific, 40% drilled in the Sea of Japan and its surrounding basins, and the
147 remaining 10% cored within the Southern Ocean and around the Antarctic Peninsula. The
148 geographic location, ocean depth, and lithology of sediments recovered at the sites are
149 provided in Table 1. The study sites represent exceptional depositional environments with
150 highly porous biosiliceous uppermost sediments that shift abruptly to less permeable
151 lower porosity units deeper in the sediment following silica diagenesis (Varkouhi, 2018).

152 A few of the study sites are located beneath the largest and most intense zone of
153 equatorial upwelling on Earth (Sites 846, 847, 1225, and 1226). This is of significance as
154 the equatorial eastern rims of the North and South Pacific Ocean were some of the major

https://doi.org/10.5194/os-2019-121
Preprint. Discussion started: 3 January 2020

Ocean Science
Discussions
Open Access
EGU

155 depocentres of biogenic silica during the Middle Miocene to Early Pliocene (Ingle, 1980,
156 1981; Behl, 1999). In 15 of the chosen sites, biogenic opal is deposited with fine detrital
157 (siliceous oozes that are accompanied by clay, silt, and sometimes volcanic ash). Though
158 detrital-based, fractions of calcareous nannofossils (and sometimes foraminifers) are
159 admixed with the diatomaceous sediment in Sites 798, 1016, 1022, 1165, 1175, and 1208.

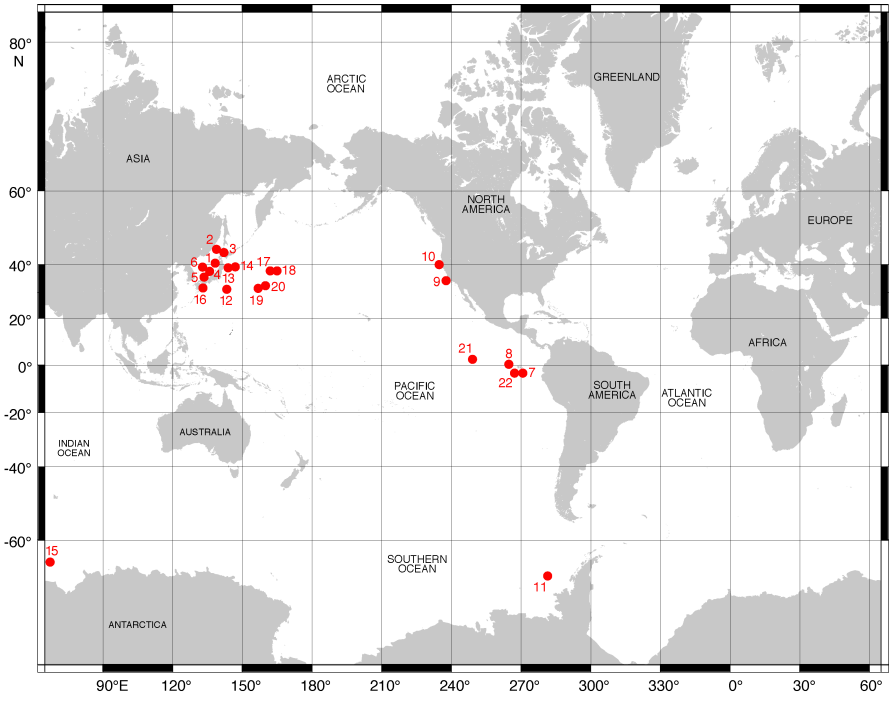

160 Figure 1. Location of the investigated ODP borehole sites (redrawn and modified from
161 Ocean Drilling Program Site Maps, 2009).

162 ODP sites (red circles): 1) 794/Leg 127, 2) 795/Leg 127, 3) 796/Leg 127, 4) 797/Leg
163 127, 5) 798/Leg 128, 6) 799/Leg 128, 7) 846/Leg 138, 8) 847/Leg 138, 9) 1016/Leg 167,
164 10) 1022/Leg 167, 11) 1095/Leg 178, 12) 1149/Leg 185, 13) 1150/Leg 186, 14)
165 1151/Leg 186, 15) 1165/Leg 188, 16) 1175/Leg 190, 17) 1207/Leg 198, 18) 1208/Leg
166 198, 19) 1211/Leg 198, 20) 1212/Leg 198, 21) 1225/Leg 201, and 22) 1226/Leg 201.

https://doi.org/10.5194/os-2019-121
Preprint. Discussion started: 3 January 2020

Ocean Science
Discussions
Open Access
EGU

167 Table 1. Description of ODP sites investigated in this study, including latitude and longitude, water depth, geographic location, and
168 description of the first lithologic unit. No. = the identification number of the ODP sites as presented in Figure 1.

No.	Site/Leg	Latitude	Longitude	Water depth, m	Geographic location	Sediment type
1	794/127	40° 11.41´N	138° 13.86´E	2822	Yamato Basin, southeastern Japan Sea	Clay and silty clay with a significant admixture of vitric ash
2	795/127	43.99°N	138.97°E	3310	Japan Sea	Silty clay with subordinate diatom clay, ashy clay, and diatom ooze
3	796/127	42.89°N	139.41°E	2596	Japan Sea	Diatom-bearing clay and silty clay
4	797/127	38.62°N	134.54°E	2876	Yamato Basin, south-central Japan Sea	Clay and silty clay with a minor admixture of vitric ash and diatoms
5	798/128	37.04°N	134.8°E	911	Oki Ridge, southeastern Japan Sea	Clay, silty clay, and diatom clay with occurrence of calcareous nannofossils and foraminifers
6	799/128	39° 22.05´N	133° 86.69´E	2985	Yamato Rise, Japan Sea	Diatomaceous ooze and diatomaceous clay with carbonate and siliciclastic sands
7	846/138	3° 5.7´S	90° 49.08´W	3387	Galapagos Islands, equatorial Pacific	Nannofossil ooze, diatom nannofossil ooze, nannofossil diatom ooze, and clayey diatom ooze
8	847/138	0° 11.59´N	95° 19.23´W	3346	Galapagos Islands, equatorial Pacific	Diatom nannofossil ooze and nannofossil ooze with minor amounts of radiolarians and foraminifers
9	1016/167	34° 32.42´N	122° 16.59´W	4162	Point Conception, California	Diatom ooze with clay, diatom clay, and clayey diatom ooze, and diatom nannofossil ooze with clay
10	1022/167	40° 4.85´N	125° 20.56´W	2325	Cape Mendocino, California	Nannofossils and siliciclastic clay with diatoms
11	1095/178	66° 59.13´S	78° 29.27´W	3863	Antarctic Peninsula, Pacific margin	Diatom-bearing silty clay, silty clay, and clay with minor siliceous ooze
12	1149/185	31° 20.52´N	143° 21.08´E	5829	Nadezhda Basin, northwestern Pacific	Clay with varying amounts of siliceous microfossils and volcanic grains
13	1150/186	39° 10.91´N	143° 19.92´E	2692	Japan Trench, off northeast Japan	Diatom ooze and diatom clay with tephra
14	1151/186	38° 45´N	143° 20´E	2182	Japan Trench, off northeast Japan	Diatomaceous silty clay with occurrence of sand, silt, and pumice as minor lithologies
15	1165/188	64° 22.22´S	67° 13.14´E	3549	Prydz Bay, Antarctic Ocean	Transition from diatomaceous ooze to diatom clay
16	1175/190	32.6°N	134.64°E	3024	Nankai Trough, southwestern Japan	Nannofossil-rich hemipelagic mud
17	1207/198	37° 47.43´N	162° 45.05´E	3112	Shatsky Rise Northern High, northern Pacific	Nannofossil ooze and clayey nannofossil ooze
18	1208/198	36° 7.63´N	158° 12.1´E	3346	Shatsky Rise Central High, northern Pacific	Alternation of nannofossil clay and ooze with siliceous tests
19	1211/198	32° 0.13´N	157° 51´E	2907	Shatsky Rise Southern High, northern Pacific	Alternation of nannofossil clay and nannofossil ooze
20	1212/198	32° 26.90´N	157° 42.70´E	2681	Shatsky Rise Southern High, northern Pacific	Nannofossil ooze with clay
21	1225/201	2° 46.25´N	110° 34.29´W	3772	East Pacific Rise	Alternation of nannofossil ooze and diatom- and radiolarian-rich nannofossil ooze
22	1226/201	3° 5.67´S	90° 49.08´W	3297	East equatorial Pacific	Alternation of diatom-rich nannofossil ooze and nannofossil-rich diatom ooze

https://doi.org/10.5194/os-2019-121
Preprint. Discussion started: 3 January 2020

Given that the sample sites reflect deep-sea zones (excluding Site 798 with a water depth of 911 m, the depths range between ~2200 and ~5800 m; Table 1), the surface sediments are not reworked nor disturbed by tidal currents and storms (Oehler, 2014). Further, sediment gravity flows did not affect the uppermost sediments at the cored sites (Shipboard Scientific Party, 1990a). Therefore, the accumulated sediment, silica dissolution, and subsequent benthic fluxes from the pore water reflect processes in the overlying water column (e.g., primary production or opal rain arriving at the seafloor). In addition, macrofaunal irrigation is thought to be only a minor effect on benthic solute-exchange fluxes at these sites (after Meile and Van Cappellen, 2003). Even in the case of uplifted sediments at Site 798, subjected to a sudden shallowing, possible low oxygen levels in the bottom water decrease the quality of infaunal habitat (Shipboard Scientific Party, 1990b), and consequently exclude pore-water irrigation.

4 Data acquisition and methods

ODP resources (initial reports and scientific results) and the IODP (International Ocean Discovery Program) databank provided the mineralogy, temperature, pore-water silica concentration, and physical properties (in particular porosity and density) for the surface and uppermost sediments of the 22 borehole sites selected for this study. The baseline information acquired during the ODP cruises through downhole and onboard-ship measurements and measurements on water and core samples is available through open access (see International Ocean Discovery Program, 2018).

The various sediment and water measurements used in this work are described in ODP

https://doi.org/10.5194/os-2019-121
Preprint. Discussion started: 3 January 2020

technical notes (Rabinowitz and Garrison, 1985; Mazzullo and Graham, 1988; Gieskes et al., 1991; Fisher and Becker, 1993; Blum, 1997). Below, a description is given for ODP methodology toward the sediment parameters reported in this study (Table 2).

In situ temperatures were measured using an APC (advanced hydraulic piston core) tool designed to assess the bottom-sediment temperature during the process of cutting a hydraulic piston core. The APC was held in place for at least 15 minutes to obtain enough data to extrapolate to *in situ* sediment temperatures (Fisher and Becker, 1993).

Once on deck, whole-round 10-cm-long samples for pore-water analyses were quickly removed from the 1.5-m-long core sections, re-capped, and sent to a cold laboratory, where they were extruded at 3°C (Mazzullo and Graham, 1988). Interstitial-water core samples were then squeezed until a sufficient quantity of water was extracted, ~10 ml from a 200 cm^3 sample. Silica concentration was determined in the pore waters by onboard ship colorimetry and analytical techniques described by Gieskes et al. (1991). As silica concentrations are temperature sensitive, the preparation and analysis of the samples under cold laboratory conditions during ODP practices ensured offsets from the actual *in situ* values were minimal.

An accurate definition of the sediment-water silica concentration gradient using ODP data to calculate sediment-water exchange rates may be argued as drilling would obscure the location of the centimetre-scale sediment-water boundary. The authors acknowledge the attenuation from saturation levels to the bottom-water value within this thin surface

https://doi.org/10.5194/os-2019-121
Preprint. Discussion started: 3 January 2020

210 sediment cannot be captured using ODP cores. However, this study used the saturation
211 value mostly from the middle and bottom of the 1-1.5 m long topmost cores (ranging in
212 depth from 0.6 to 1.3 mbsf), which is well within the depth realm of marine benthic layer.
213 The benthic layer is defined, by following Wildish (2001), as an ecological zone at the
214 lowest level of seawater column which thickness varies from 10 cm to 5 m and includes
215 benthic substrate and the topmost sediment layer. This typical depth zone (0.6 to 1.3
216 mbsf) is strongly influenced by benthic sediment-water interactions, particularly diffusion
217 which leads to a developed silica concentration gradient from this point to the bottom
218 water (Hurd, 1973). More importantly, most changes in silica concentration occur within
219 30-40 cm of the surface of sediment, and from this depth downwards to l-2 mbsf the
220 concentration commonly becomes constant (e.g., Van Cappellen and Qiu, 1997a; Van der
221 Weijden and Van der Weijden, 2002). Therefore, silica concentration from the topmost
222 core still represents the saturation value for a few tens of centimetres of sediment surface.

223 Multi-sensor track logged the 1.5-m-long cores for gamma ray density, compressional
224 wave velocity, magnetic susceptibility, and natural gamma radiation. Specimens were
225 extracted from the cores for measuring the moisture and average mineral density (MAD)
226 (Blum, 1997). From these measurements, basic physical properties, including porosity,
227 bulk density, grain density, dry density, and void ratio were calculated.

228 Smear slides of unconsolidated sediments were prepared to document the lithology of
229 recovered material and to describe the cores. A visual estimation technique, using
230 comparator charts of Terry and Chilingarian (1955), was applied by ODP to determine

https://doi.org/10.5194/os-2019-121
Preprint. Discussion started: 3 January 2020

231 the relative percentages of minerals, skeletal grains, and other sediment components. The
232 composition of the surficial sediments was derived from results of this approach.

233 Dissolution rates and benthic effluxes of dissolved silica and the burial fluxes of opal
234 were calculated and modelled based on the sediment parameters described above. In the
235 following section, equations required for these calculations are introduced.

236 4.1 Early diagenetic equations for silica

237 A first-order kinetic rate law (Equation 1.1) is the most widely used expression for the
238 dissolution of biogenic opal. This relates the dissolution rate to a linear function of the
239 degree of pore-water undersaturation with respect to opal. The term $1\text{-}C/C_{sat}$ ($0 \leq C/C_{sat} <$
240 1) in Equation (1.1) represents the degree of undersaturation with dissolving silica.

241 Whether stated explicitly or not, it is typically assumed that C in Equation 1.1 is equal to
242 the bottom-water silicic acid concentration. The C_{sat} equates to the near constant
243 concentration of dissolved silica at depths a few centimetres, usually < 10 cm below the
244 sediment surface, and represents the equilibrium solubility of deposited biogenic silica
245 (i.e., asymptotic silica concentration or saturation concentration).

246 Temperature dependence on the kinetic rate constant is typically expressed using the
247 Arrhenius' Law (1889):

248 $$k = Ae^{\frac{-Ea}{RT}} \quad (1.2)$$

https://doi.org/10.5194/os-2019-121
Preprint. Discussion started: 3 January 2020

where A is the pre-exponential factor (in s^{-1}), E_a is the apparent activation energy of the dissolution reaction (in J mol^{-1}), R is the universal gas constant (8.314 J K^{-1} mol^{-1}), and T is absolute temperature (in K).

Temperature controls the kinetic rate constant through interaction with activation energy to initiate the silica dissolution reaction (Dralus et al., 2015). This allows for basic predictions toward variations in the dissolution rate coefficient with temperature. The exponent E_a/RT is the ratio of the activation energy to the average kinetic energy (RT) and as this ratio increases (with consideration of the negative sign behind it), the coefficient increases. This implies higher temperatures, while other parameters in the equation kept constant, favour larger rate coefficients; thus speeding up the reaction. Although a narrow range of variations for modern seafloor temperatures imposes slight changes in rate coefficients, their effects on reaction kinetics is substantial due to exponential variability of silica saturation with temperature (Williams and Crerar, 1985).

The mathematical expansion of Equation 1.1 combined with the Fick's diffusion law yields an expression for the benthic flux of silica (Dixit and Van Cappellen, 2003):

$$J_0 = \left(kM_{opal}C_{sat}D_s\phi\left(1-\phi\right)\rho_b\right)^{0.5}\left(1-\frac{C_{bw}}{C_{sat}}\right) \qquad (1.3)$$

where J_0 is the benthic flux of silicic acid (in mol m^{-2} yr^{-1}), k is the first-order rate coefficient (for Equation 1.3, the unit is converted from s^{-1} into yr^{-1}), M_{opal} is particulate biogenic silica concentration (in volume %), D_s is the sediment diffusion coefficient (in

https://doi.org/10.5194/os-2019-121
Preprint. Discussion started: 3 January 2020

268 m^2 yr^{-1}), Φ is the sediment porosity (in %), ρ_b is the grain density of the sediment (in kg m^{-3}), C_{bw} is the bottom-water dissolved silica concentration (in µM), and C_{sat} is the asymptotic silica concentration (saturation concentration) (in µM).

271 Although based on a simplified model of silica diagenesis, Equation 1.3 incorporates the main properties and variables of the early diagenetic system that affect the benthic fluxes of dissolved silica diffused from marine sediments back to the seawater.

274 The fraction of the opaline rain flux that reaches the water-sediment interface and that is neither dissolved nor diffused back to the water column is then buried within the sediment. This burial flux of biogenic silica is estimated using the mass accumulation equation (after Oehler, 2014):

278 $$BSi_{acc} = M_{opal}\omega\left(1-\phi\right)\rho_b \qquad (1.4)$$

279 where BSi_{acc} is the accumulation rate of biogenic silica within the sediment (in kg m^{-2} yr^{-1}), M_{opal} is the amount of biogenic silica (in volume %), ω is sedimentation rate (in m yr^{-1}), Φ is the sediment porosity (in %), and ρ_b is the sediment density (kg m^{-3}).

282 The rain rate of opal arriving at the seabed can then be calculated using the silica mass balance equation (Rabouille et al., 1997; Ragueneau et al., 2009):

284 $$BSi_{rain} = J_0 + BSi_{acc} \qquad (1.5)$$

https://doi.org/10.5194/os-2019-121
Preprint. Discussion started: 3 January 2020

where BSi_{rain} is the rain rate of biogenic silica reaching the seafloor (in mol m^{-2} yr^{-1}), J_0 is the diffusive flux of silicic acid at water-sediment interface (in mol m^{-2} yr^{-1}), and BSi_{acc} is the accumulation rate of opal in the sediment (for Equation 1.5, the accumulated biogenic silica is converted from kg m^{-2} yr^{-1} into mol m^{-2} yr^{-1}).

5 Results

5.1 ODP-derived dataset

The sediment composition, bottom-water temperatures, pore-water silica concentrations, and the results of sediment porosity and density measurements for the 22 study sites are reported by the ODP. To calculate opal dissolution rates as well as benthic and burial fluxes, a dataset composed of these parameters was assembled for the chosen sites (Table 2). The lithology of the unit accommodating biogenic opal within the topmost sediment layers was categorised into two groups: detrital and carbonate. Almost 70% of the surface sediment layers are hosted by detrital lithologies; the others by biogenic carbonate.

Modifying the ODP approach for partitioning the sediment components (Marsaglia et al., 2013), sediment sample composition was divided into three fractions: biogenic opal (consisting of diatoms, radiolarians, silicoflagellates, and sponge spicules), detrital material (composed mainly of clays, detrital quartz, oxides, volcanic ash, and volcanic glass), and biogenic carbonate (calcareous nannofossils and foraminifers). When combined with accessory particles (organic debris, plant debris, and accessory minerals), the total is 100% for solid sediment volume. The sediments exhibit a wide compositional range. Biogenic silica content varies from 5 to 71%, detrital from 0 to 91%, and biogenic

https://doi.org/10.5194/os-2019-121
Preprint. Discussion started: 3 January 2020

Ocean Science
Discussions
Open Access
EGU

306 Table 2. Dataset assembled from the ODP data sources for the uppermost sediment of the
307 22 study sites. No. = the identification number of the ODP sites presented in Figure 1,
308 M_{opal} = biogenic silica content of the uppermost sediment layer, T = present-day *in situ*
309 bottom-water temperature, C_{bw} = bottom-water concentration of silicic acid, C_{sat} =
310 asymptotic pore-water concentration of silicic acid, Φ = porosity of the uppermost
311 sediment layer, ρ_b = grain density of the uppermost sediment layer, D_s = diffusion
312 coefficient of sediment, and ω = sedimentation rate of the lithologic unit hosting the
313 uppermost sediment layer. With the exception of C_{bw} values for Sites 794 through 799
314 that were extracted from Sarmiento et al. (2007), all other values in the table were
315 obtained from the ODP.

No.	Site	Host [a] lithology	M_{opal}, %	Detrital, [b] %	Carbonate, [b] %	T, K	C_{bw}, µM	C_{sat}, µM	Φ, %	ρ_b, kg m^{-3}	$D_s \times 10^{-10}$, [c] m^2 s^{-1}	$\omega \times 10^{-5}$, m yr^{-1}
1	794	Detrital	15	84	0	273.36	70	440	85	2660	3.97	3.5
2	795	Detrital	15	83	0	273.35	70	615	93	2550	4.76	4.8
3	796	Detrital	7	91	0	273.15	70	740	77	2500	3.26	7.4
4	797	Detrital	10	89	0	273.35	70	540	81	2620	3.61	4.6
5	798	Detrital	17	75	7	274.55	60	620	77	2360	3.26	12.2
6	799	Detrital	29	65	3	273.29	70	537	88	2700	4.26	7.1
9	1016	Detrital	20	69	9	274.45	170	804	80	2770	3.52	5.3
10	1022	Detrital	5	83	10	275.05	160	702	65	2750	2.32	10.1
11	1095	Detrital	10	88	0	273.34	140	380	74	2730	3.01	2.2
12	1149	Detrital	21	76	2	274.21	190	559	81	2680	3.61	3.4
13	1150	Detrital	65	32	2	275.29	140	550	83	2420	3.79	20.5
14	1151	Detrital	33	63	3	275.26	140	500	77	2700	3.26	7.2
15	1165	Detrital	71	20	8	272.85	140	522	75	2700	3.09	1.5
16	1175	Detrital	15	74	10	274.77	140	556	67	2640	2.47	52
18	1208	Detrital	15	53	30	274.3	160	726	80	2670	3.52	4.2
7	846	Carbonate	39	5	55	274.96	160	892	84	2490	3.88	4
8	847	Carbonate	27	6	65	274.95	160	901	85	2700	3.97	3.2
17	1207	Carbonate	17	29	53	274.4	160	584	73	2690	2.93	1.4
19	1211	Carbonate	14	20	64	274.2	160	540	66	2690	2.4	0.9
20	1212	Carbonate	10	26	63	274.25	160	552	70	2710	2.7	1.4
21	1225	Carbonate	32	1	66	274.55	160	625	78	2700	3.35	8.9
22	1226	Carbonate	51	0	49	274.85	160	772	84	2580	3.88	4

316 [a] Lithological composition of the sediment hosting biogenic silica.
317 [b] Detrital (in percent of total volume) and biogenic carbonate (in percent of total volume)
318 components of the topmost sediment layer.
319 [c] Diffusion coefficient of sediment determined using equation $D_s = \Phi^2 \times D$ (Ullmann and
320 Aller, 1982), where Φ is the porosity value (derived from the ODP database), and D (5.5
321 $\times 10^{-10}$ m^2 s^{-1}; Rickert, 2000) is the free-solution molecular diffusion coefficient for silicic
322 acid.

https://doi.org/10.5194/os-2019-121
Preprint. Discussion started: 3 January 2020

carbonate from 0 to 66%. The obtained values for accessory particles are not provided (Table 2). Given the research aims, the lithologic composition of the sites was divided into two categories; detrital and carbonate. On this basis, the detrital-dominated sites having a mean of 70% detrital matter contain on average 23% biogenic silica and only 5% carbonate. Conversely, the carbonate-dominant sites having a mean carbonate mineral content of 60% include an average of 12% detrital material and 27% opal. The highest contribution of biogenic opal to the sediment composition is reported from the detrital-based Site 1165 in the Southern Ocean. This site is situated at a sub-polar latitude beneath a major upwelling zone where there are high rates of opal rain. Relatively lower rates of detrital particle rain account for high concentration of solid opaline silica in the surficial sediments (after Rashid, 1985; Libes, 1992). The highest detrital matter content is reported from Sites 796 and 797 in the Sea of Japan and Yamato Basin, respectively, where clay particles are the principal constituent of detrital sediment, formed through chemical alteration of either windblown volcanic ash or volcanic glass on the seafloor, in addition to products of continental weathering from the source region. The highest biogenic carbonate content is reported from Site 1225 in the Eastern Pacific Rise where nannofossil oozes alternate with layers rich in diatoms and radiolarians.

The present-day low temperature at the water-sediment interface for the chosen sites varies from 272.85 to 275.29 K. The maximum temperature was recorded in the deep-sea terrace of the Japan Trench (Site 1150), where heat flow is anomalously high, averaging 60–70 mW/m^2, appreciably higher than typical heat flows for seafloors aged 135 Ma. The probable cause of the higher bottom-water temperature at this site is an efficient vertical

https://doi.org/10.5194/os-2019-121
Preprint. Discussion started: 3 January 2020

heat transport by hydrothermal circulation within a permeable layer in the oceanic crust, developed by fracturing due to plate bending (Yamano et al., 2014). The lowest temperature was recorded in diatom ooze to diatom clay of Prydz Bay in the Antarctic.

The bottom-water silica concentrations vary from 60 to 190 µM, with the maximum values observed in the uppermost sediments of the Nadezhda Basin in the northern Pacific. Minimum values are found in the Sea of Japan. The asymptotic silicic acid concentrations of sediments range from 380 to ca. 900 µM. These values compare well with the silica concentration levels of benthic chambers reported from other ocean basins (e.g., see Rabouille et al., 1997) . The highest values are observed in diatomaceous nannofossil oozes of the Galapagos Islands in the equatorial Pacific, the lowest in the diatom-bearing fine detrital sediments of the Antarctic Peninsula. However, even within the same oceanic region the silica asymptotic concentration can vary widely. For instance, in the Sea of Japan, concentrations differ by as much as 300 µM.

Porosity and sediment grain densities vary between 65 and 93% and 2360 to 2770 kg m^{-3}, respectively. The highest benthic porosity is observed in the surficial silty clay sediments of the Japan Sea that contain subordinate diatom clay and diatom ooze. Grain density is highest in the diatomaceous ooze containing clay, diatom clay, diatom ooze, and diatom nannofossil ooze from the western Point Conception in California.

The sediment diffusion coefficient, scaled with tortuosity according to the equation $D_s = \Phi^2 \times D$ (Table 2), varies from 2.32×10^{-10} to 4.76×10^{-10} m^2 s^{-1}, with the peak value

https://doi.org/10.5194/os-2019-121
Preprint. Discussion started: 3 January 2020

365 associated with the silty clay sediments of Site 795 in the Sea of Japan. Because of a very
366 narrow range of bottom-water temperatures (2.44 K), correction of seawater molecular
367 diffusion coefficient for temperature was omitted in this study and a value of 5.5×10^{-10} m^2
368 s^{-1} was adopted as representative of the free-solution diffusion coefficient for dissolved
369 silica. The estimated sedimentation rates range between 0.9×10^{-5} and 20.5×10^{-5} m yr^{-1},
370 with the highest rates observed for the diatom ooze and clay deposits in Japan Trench.
371 The lowest rates are for the nannofossil clay and ooze from the Southern High of Shatsky
372 Rise in northern Pacific (Sites 1211 and 1212).

373 **6 Discussion**

374 6.1 Model parameters: Calibration

375 One of the problems in the modelling of the early diagenesis of silica is the kinetic
376 coefficient *k* of opal dissolution that is poorly constrained and commonly used as a fitting
377 parameter in the diagenetic models (Dixit and Van Cappellen, 2003). The kinetic
378 coefficients obtained through fitting of pore-water profiles vary greatly between different
379 sediments (e.g., Schink et al., 1975). This is usually due to differences in temperature and
380 the mineralogical nature of the sediments. To limit such a marked variability, the kinetic
381 rate constant has been adjusted separately for each studied ODP site using the site-
382 specific bottom-water temperatures, a common activation energy of approximately 50 KJ
383 mol^{-1} (50000 J mol^{-1}) for the dissolution of biogenic silica (following Dove and Rimstidt,
384 1994; Van Cappellen and Qiu, 1997b) and a first-order pre-exponential factor of ~30 s^{-1}.
385 The linear variability of adjusted kinetic coefficient values due to differences in modern
386 bottom-water temperatures (Fig. 2) deviates from the general trend of an exponential

https://doi.org/10.5194/os-2019-121
Preprint. Discussion started: 3 January 2020

387 relationship with temperature for the solubility of silica. This is related to the narrow
388 range of low seafloor temperatures (272.85–275.29 K), the presence of detrital matter in
389 most sediments (this puts a constraint on the dissolution kinetics of opal), and a common
390 activation energy set for dissolution of opal within the benthic layer of investigated sites.

391 Observed variations in the asymptotic concentrations C_{sat} of silicic acid across the study
392 sites poses another challenge for modelling the early diagenesis of silica. Despite
393 temperature differences across the water-sediment interface and large variations in the
394 asymptotic concentrations of dissolved silica, even where the lithologic composition of
395 biosiliceous sediments is very similar, the relationship between C_{sat} and bottom-water
396 temperature (T) remains robust across the range of deep-sea environments, especially
397 across the carbonate-hosted settings included in this study (Fig. 3). This relationship was
398 therefore used to calibrate the C_{sat} against sediment temperature when calculating the
399 dissolution rate and benthic flux of silica through Equations 1.1 and 1.3, respectively.

400 Empirical equations relating C_{sat} to the T values in clay- and carbonate-hosted sites fitted
401 through the data points (representing the regression lines in Figure 3) are:

402 $C_{sat} = 3.607 \times 10^{-5} e^{0.0605T}$ $R^2 = 0.1$, for detrital-hosted sediments, and
403 $C_{sat} = 1.101 \times 10^{-77} e^{0.669T}$ $R^2 = 0.97$, for carbonate-hosted sediments

404 where C_{sat} is expressed in µM.

https://doi.org/10.5194/os-2019-121
Preprint. Discussion started: 3 January 2020

Ocean Science
Discussions
Open Access
EGU

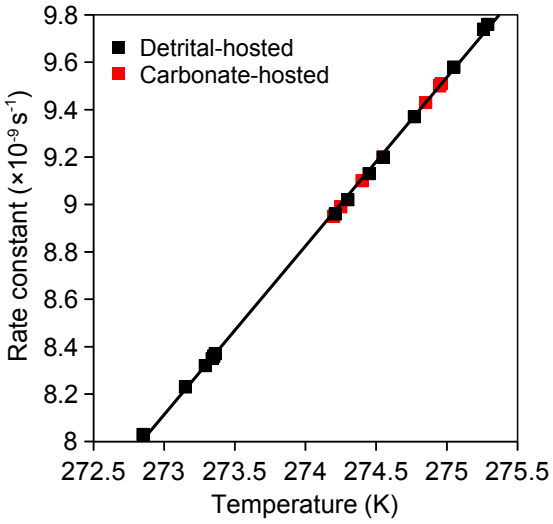

405 Figure 2. The first-order variability of dissolution rate coefficient with bottom-water
406 temperature at the detrital- and carbonate-hosted 22 selected ODP sites. The rate constant
407 values were calculated using the Arrhenius' (1889) equation.

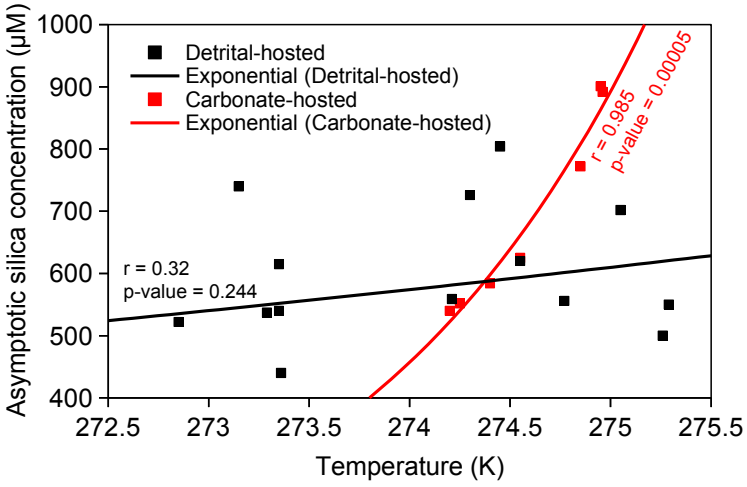

408 Figure 3. Asymptotic silicic acid concentration as a function of present-day temperature
409 of the clay- and carbonate-based surface sediments. The p-value (< 0.05, according to
410 Noymer, 2008) shows the relationship between the data points for carbonate sediments is
411 more significant than that for detrital sediments.

https://doi.org/10.5194/os-2019-121
Preprint. Discussion started: 3 January 2020

412 The exponential best fit overpredicted the ODP-reported asymptotic concentrations of
413 silicic acid in the clayey sediments of Yamato Basin by as much as 9 µM. The best fit for
414 carbonate-hosted sediments predicted very well (only 0.5 µM overprediction) the
415 concentrations measured by the ODP for nannofossil oozes from the Northern High of
416 Shatsky Rise in the northern Pacific Ocean.

417 6.2 Dissolution rate and benthic efflux: Empirical models

418 Dissolution rates for biogenic opal and the benthic fluxes of produced dissolved silica
419 were predicted through the diagenetic equations 1.1 and 1.3, respectively. Values of solid
420 opal content, porosity, density, and the diffusion coefficient of the uppermost sediment
421 layer as well as the bottom-water and asymptotic concentrations for silicic acid were
422 taken from Table 2. The asymptotic concentrations from Table 2 were calibrated based
423 on empirical relationships defined in Figure 3, and the values of site-specific kinetic rate
424 constants were based on the Arrhenius Law.

425 Two different scenarios were used to calculate the dissolution rate and benthic efflux of
426 biogenic silica. In the first scenario, the normalised asymptotic silicic acid concentration
427 (C^*_{sat}) was kept constant and values were set as equal to the estimated peak amounts
428 within the uppermost sediments of Sites 1150 and 846 for clay and carbonate host
429 sediments, respectively. This scenario thus assumes that the thermodynamic properties of
430 sedimentary biogenic silica are unaffected by the present-day temperature and
431 composition of the sediment. As far as silica dissolution is concerned, bottom-water
432 temperatures vary across the sites, and the sediments differ by their contents of detrital,

https://doi.org/10.5194/os-2019-121
Preprint. Discussion started: 3 January 2020

433 carbonate, and biogenic opal (Table 2). In the second scenario, the asymptotic
434 concentration depends on the temperature, implying that the increase in C^*_{sat} (and also k)
435 with observed increases in bottom-water temperatures (Figs. 2 and 3) follows the
436 common dependency observed through laboratory experiments for samples recovered
437 from different basins (e.g., Rabouille et al., 1997; Van Cappellen and Qiu, 1997a). The
438 second scenario best represents the effect of bottom-water temperature on the dissolution
439 and efflux of silica during early diagenesis (Figs. 4 and 5). When thermodynamic and
440 kinetic effects on the production of silicic acid are considered, a better association is
441 observed between the predicted dissolution rate and diffusive flux and temperature. A
442 slight increase in dissolution rates and benthic fluxes with temperature for detrital-based
443 sediments—as compared with a significant increase in carbonate sites for both scenarios
444 —strongly suggests the rate-limiting effects of the presence of detrital matter in the
445 sediment. The incorporation of fine detritus into the external layer of biosiliceous tests
446 significantly alters their solubility and reactivity. The transition from a linear to an
447 exponential increase of the dissolution rate and flux values in carbonate-based sediments
448 when shifting from the first to the second scenario is because the variability in saturation
449 levels of silica is involved in the early diagenetic reactions.

450 The dissolution rates and benthic fluxes predicted from the second scenario were
451 recalculated separately for two host sediment types assuming average values for porosity,
452 density, and bottom-water silica concentrations (average Φ, ρ_b, and C_{bw} in detrital-hosted
453 sediments being 80%, 2600 kg m^{-3}, and 120 µM, respectively; carbonate-hosted sediment
454 had average values of 77%, 2650 kg m^{-3}, and 160 µM for Φ, ρ_b, and C_{bw}, respectively).

https://doi.org/10.5194/os-2019-121
Preprint. Discussion started: 3 January 2020

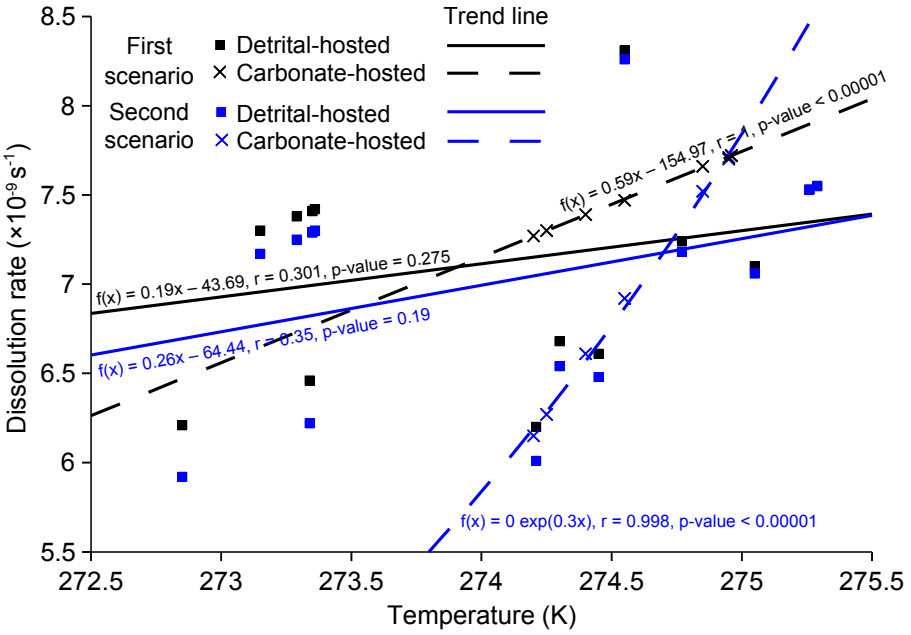

455 Figure 4. Calculated dissolution rate of sedimentary biogenic opal versus bottom-water
456 temperature for the investigated sites. Note the difference between the rate variabilities
457 with temperature, particularly for the carbonate-hosted sites, when shifting from the first
458 (constant calibrated asymptotic concentration of silica) to the second scenario
459 (asymptotic concentration varies with temperature). The p-values (< 0.05, Noymer, 2008)
460 show the dissolution rate-temperature relation in carbonate-dominated sites for both
461 scenarios is more significant than that for detrital-dominated sites. These values also
462 indicate that the correlation between the data points is more significant in the second
463 scenario than the first scenario.

464 The dissolution rates calculated with the average parameter values in carbonate sites
465 match perfectly those calculated with the site-specific values reported in Table 2 (Fig. 6).
466 This occurs as bottom-water silicic acid concentrations remain constant among all the
467 carbonate-based sites. However, for detrital-dominated sites, based on: 1) an observed

https://doi.org/10.5194/os-2019-121
Preprint. Discussion started: 3 January 2020

468 shift from a weakly positive correlation between dissolution rates and temperature to a
469 strong linear correlation for the properties, and 2) recalculation of dissolution rates using
470 average values produces rates that are generally higher than for site-specific values, a
471 strong case can be made that variations in the pore-water concentrations of dissolved
472 silica is an important source of variability for the dissolution rate of biogenic opal.

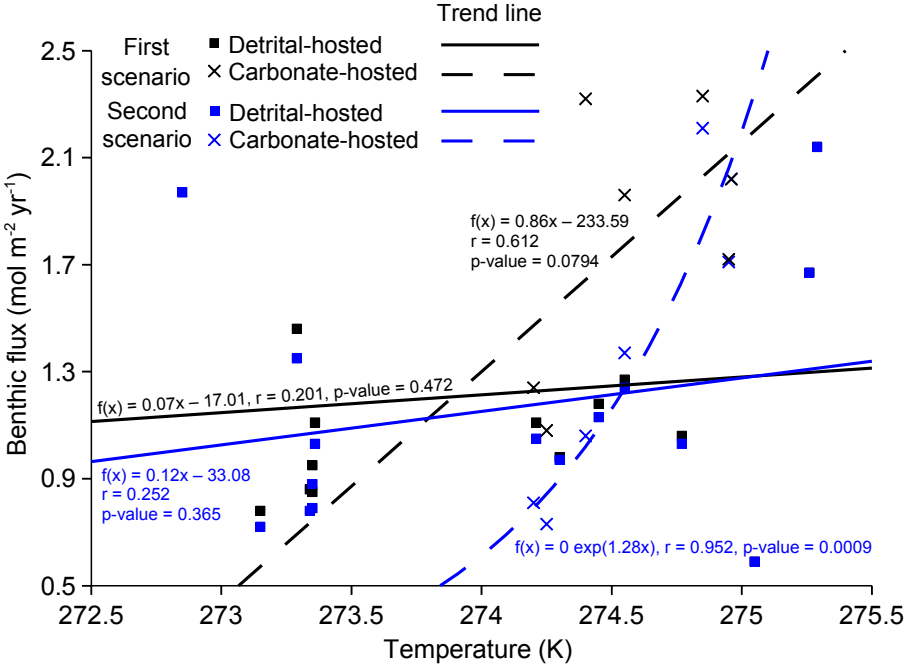

473 Figure 5. Calculated benthic flux of silicic acid versus bottom-water temperatures at the
474 investigated ODP sites. Note the variability of flux, particularly for carbonate-hosted
475 sites, when shifting from the first scenario (constant asymptotic concentration of silica) to
476 the second scenario (site-specific asymptotic silica concentration). The p-values show the
477 relationship between the data points for carbonate-dominated sites for both scenarios is
478 statistically more significant than that for detrital sites. These values also show the
479 correlation between the data points for the second scenario is more significant than that
480 for the first scenario.

https://doi.org/10.5194/os-2019-121
Preprint. Discussion started: 3 January 2020

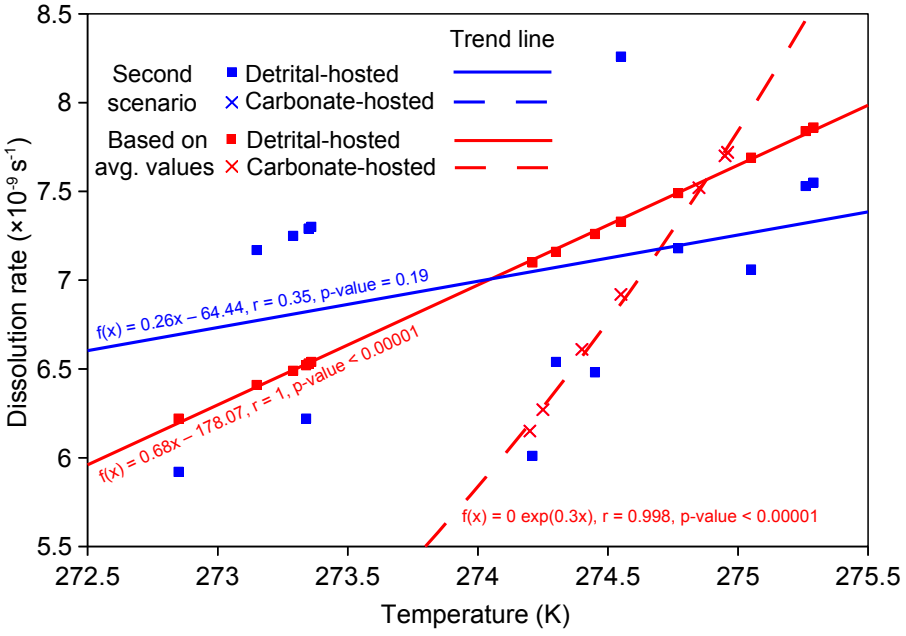

481 Figure 6. Dissolution rates of biogenic silica as a function of bottom-water temperature at
482 the investigated sites. Note a transition from a weak positive correlation to a strong
483 positive linear correlation at the clay-hosted sites when shifting from rate values
484 calculated based on the second scenario (variable asymptotic concentration of silica with
485 temperature) to those calculated using average parameter values (average bottom-water
486 silica concentration). The dissolution rates at the carbonate-dominated sites do not change
487 when shifting from a second scenario to those predicted based on average parameter
488 values. The p-values (< 0.05, Noymer, 2008) show the relationship between the data
489 points for carbonate-dominated sites is statistically more significant than that for detrital
490 sites. These values also show the correlation between the data points determined based on
491 average parameter values is more significant.

492 At detrital-hosted sites, the corresponding benthic fluxes predicted either using site-
493 specific parameters or using average values exhibiting a slight increase with temperature
494 (Fig. 7), highlight effects of detrital matter admixed with biogenic silica in confining the

https://doi.org/10.5194/os-2019-121
Preprint. Discussion started: 3 January 2020

495 diffusive flux of silicic acid from the seafloor. The presence of sufficient fractions of
496 detrital material (especially aluminosilicates) in the sediment causes a reduction in the
497 rate of silicic acid production under the temperature-dependent dissolution kinetics of
498 biogenic opal. This, in turn, affects the benthic flux. In such cases, variations in porosity,
499 grain density, and bottom-water silicic acid concentration can only be a subordinate
500 source of variability for benthic fluxes of silicic acid. Conversely, in carbonate sites, the
501 close correspondence between the increasing effluxes of dissolved silica, predicted using
502 either the average or site-specific parameters, shows an exponential trend. This suggests a
503 much more important role for bottom-water temperature in increasing silicic acid
504 concentrations, thereby leading to the higher benthic fluxes. In addition, appearing
505 directly from Equation 1.3, the amount of solid biogenic silica in the sediment also plays
506 a key role in the evolution of silicic acid benthic flux as k and C_{sat} are dependent on the
507 mineralogical composition of the sediment. An increase in the biogenic opal content of
508 the sediment increases the access rate of pore water to the reactive surface areas of
509 siliceous shells (even when the sediment contains detrital particles). This, in turn, helps
510 these kinetic and thermodynamic parameters of biogenic opal to actively increase under
511 the present-day bottom temperatures.

512 As inferred from Figures 6 and 7, the linear dependence on *in situ* temperatures of opal
513 dissolution rate and associated diffusive fluxes in detrital-hosted benthic layers, while
514 showing a substantial dependence on temperature in carbonate sites, are best represented
515 by the values predicted using average parameter values. Unfortunately, no measured
516 values of dissolution rates and benthic fluxes of silica are available for these study sites.

https://doi.org/10.5194/os-2019-121
Preprint. Discussion started: 3 January 2020

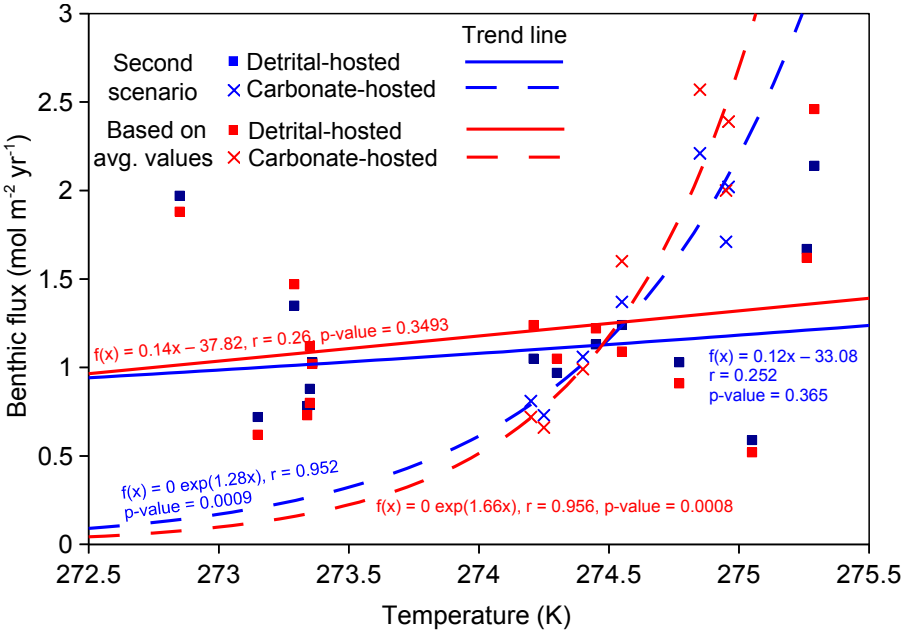

517 Figure 7. Benthic fluxes of dissolved silica as a function of bottom-water temperature at
518 the studied sites. Note the closely corresponding flux values for the detrital-hosted sites
519 when shifting from the second scenario (site-specific parameter values) to values
520 calculated based on average parameters (including average porosity, density, and bottom-
521 water silica concentration). In carbonate-hosted sites, the flux values based on average
522 parameters mimic those calculated using site-specific parameters. The p-values show the
523 relationship between the data points for carbonate-dominated sites is more significant
524 than that for detrital sites. The values also indicate that the correlation between the data
525 points determined using average values is more significant than that between the data
526 points from the second scenario.

527 Therefore, values obtained from other ocean regions were used for comparison. As seen
528 in Figures 8 and 9, the measured parameters deviate markedly from the predicted values
529 at the investigated ODP sites (except for a very few detrital-based sites clustered close to

https://doi.org/10.5194/os-2019-121
Preprint. Discussion started: 3 January 2020

530 the modelled curves for the benthic flux). This deviation, while the saturation
531 concentrations from the present study are comparable to those of other studies, is due to
532 temperature differences and large discrepancies between the composition of the
533 sediments sampled in this study and that of other works.

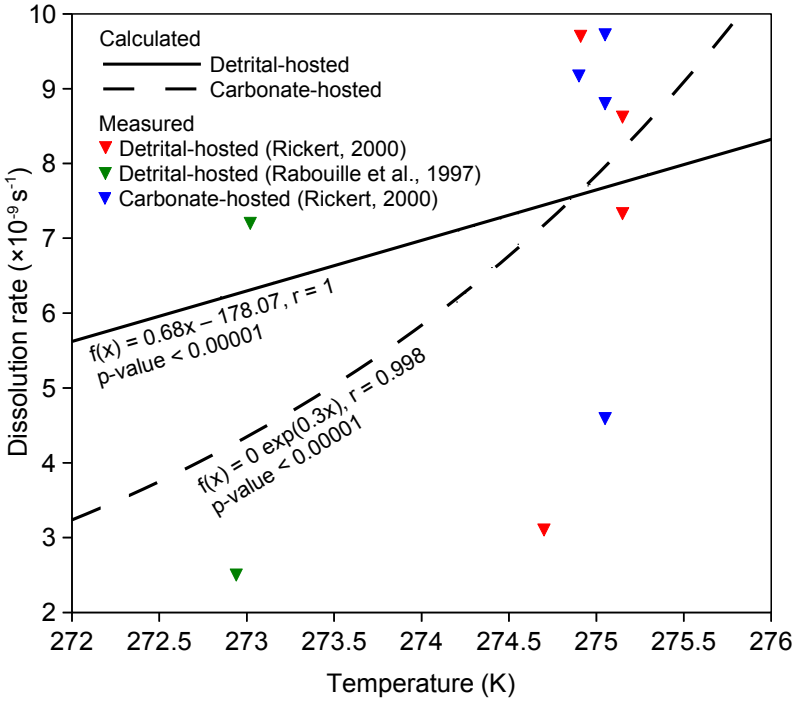

534 Figure 8. Dissolution rate of opal predicted using average parameter values versus
535 bottom-water temperature at the studied ODP sites. The linear and exponential lines
536 correspond to the model-predicted dissolution rates for detrital- and carbonate-dominated
537 host lithologies, respectively. Also plotted are the dissolution rates determined for other
538 ocean regions.

https://doi.org/10.5194/os-2019-121
Preprint. Discussion started: 3 January 2020

539 6.3 Controls on pore-water undersaturation

540 The model-predicted increased dissolution rate of opal with bottom-water temperature in
541 detrital-hosted sediments (Figs. 6 and 8) is consistent with the variability of dissolution
542 rate constant and fits well with the linear dissolution rate law. The pore-water
543 undersaturation state with respect to the dissolving opal phase within the surface
544 sediments could explain this linear pattern (Fig. 10). According to Van Cappellen and
545 Qiu (1997b), only at very high levels of undersaturation (commonly > 0.85) do the
546 dissolution kinetics of biogenic silica deviate from the linear rate law, which then
547 increases in a non-linear manner with increasing undersaturation. The high detrital to
548 opal ratios for the clay-dominated sites from this study (the mean ratio being 6; Fig. 10)
549 have, however, modified the dissolution rates significantly. The slow increase in the opal
550 dissolution rate with bottom-water temperatures in detrital-hosted sediments is attributed
551 to the complementary active role of clays, as they compete with silica dissolution for the
552 available alkalinity from ocean water (Kastner et al., 1977). As a result, aluminosilicates
553 in the sediment (especially clay minerals) provide an additional sink for the alkalinity and
554 the rate of opal dissolution is thereby reduced. Though causing lower degrees of pore-
555 water undersaturation with respect to the *in situ* solubility of biogenic silica, an elevated
556 detrital fraction in biosiliceous sediments prevents pore water from reaching equilibrium
557 with biogenic silica because it confines the maximum levels of silicic acid (Dixit et al.,
558 2001; Dixit and Van Cappellen, 2003; Martin and Sayles, 2003). Here, low bottom-water
559 temperatures act as a control that mainly influences the opal saturation state in pore-water
560 solutions by increasing silica concentrations at higher dissolution rates (according to
561 Williams and Crerar, 1985).

https://doi.org/10.5194/os-2019-121
Preprint. Discussion started: 3 January 2020

562 In carbonate sites, conversely, the dissolution of carbonate provides the required
563 alkalinity for both silica dissolution and the formation of aluminosilicates. As such, the
564 influence of clay minerals is strikingly reduced. Further, very low relative detrital
565 fractions of carbonate-hosted sediments (the mean value being 0.8; Fig. 10) have
566 significantly limited their control on silica solubility. These lead to the rapidly increasing
567 saturation concentrations of silicic acid (although pore waters remain highly
568 undersaturated with respect to opal) at low seafloor temperatures (Fig. 3), and account for
569 the transition from a linear to nonlinear exponential opal dissolution trend. Comparably,
570 the primary effect of temperature on opal in carbonate-dominated surface sediments is to
571 decrease the relative saturation degree of the pore-water with this mineral phase while
572 speeding up the rate of its dissolution.

573 Since both the dissolution rate and the benthic flux of silicic acid depend positively on
574 the present-day cold bottom-water temperatures (Figs. 4–9), a positive relationship is
575 expected between them. The model-predicted benthic fluxes confirm this expected
576 relationship (Figs. 7 and 9). Compared to the slight increases in benthic fluxes with
577 temperature at clay-dominated sites, the exponential trend of increased benthic fluxes
578 with temperature for carbonate sites is related to the higher rates of silicic acid production
579 in pore waters that are highly undersaturated with respect to biosilica.

580 The function of bottom temperature during silica early diagenesis through influencing the
581 undersaturation status with biogenic opal in pore water focused in this study seems to be
582 in contrast with the results of comparable research by Frings (2017) which, based on 453

https://doi.org/10.5194/os-2019-121
Preprint. Discussion started: 3 January 2020

583 published pore-water profiles compiled from various ocean settings worldwide, show that
584 the silica saturation concentration and its fluxes across the sediment-water interface are
585 unrelated to the present-day *in situ* temperatures. The discrepancy between these works
586 arises from significant difference between their ranges of bottom-water temperature
587 variations used to establish a relationship with the silica exchange reactions.

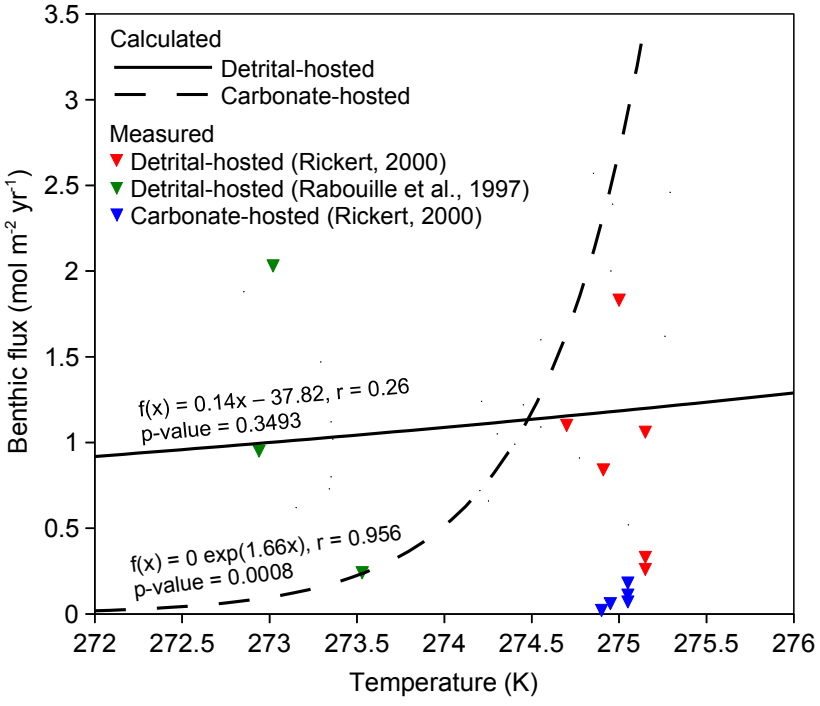

588 Figure 9. Benthic fluxes of silicic acid versus bottom-water temperature for the various
589 studied ocean regions. The lines correspond to model-predicted fluxes, calculated using
590 average porosity, density, and bottom-water silica concentrations, for clay- (solid line)
591 and carbonate-hosted (dashed line) sites. Also shown are the benthic fluxes determined
592 for other ocean basins.

https://doi.org/10.5194/os-2019-121
Preprint. Discussion started: 3 January 2020

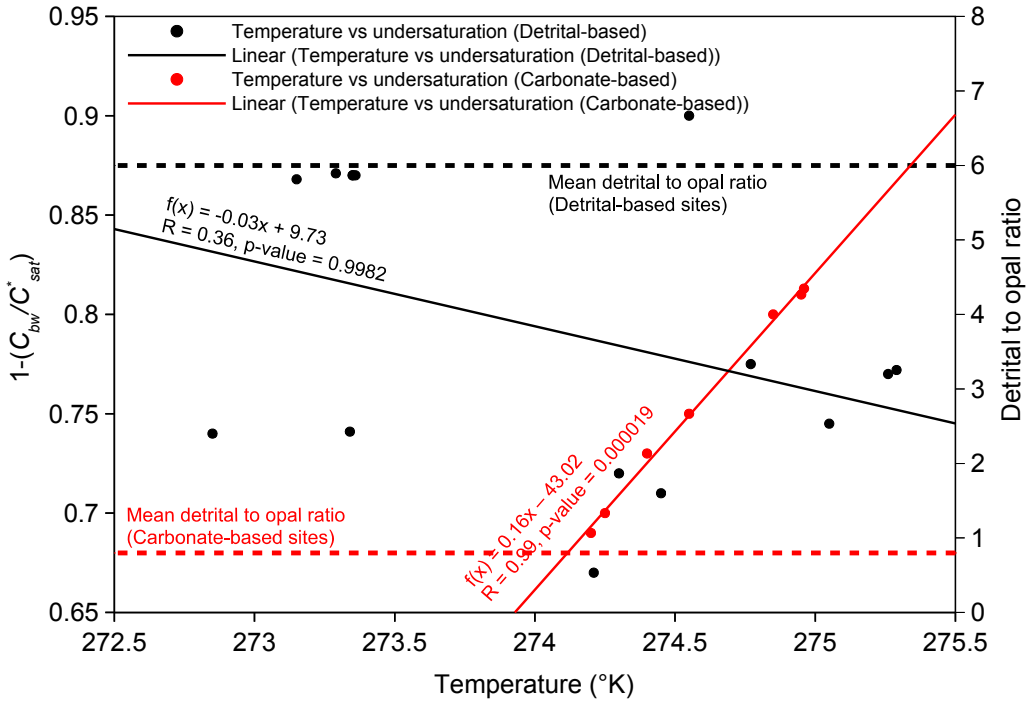

593 Figure 10. Degree of undersaturation with respect to opal versus bottom-water
594 temperature at the studied ODP sites. Also shown is the average relative detrital fraction
595 of the sediments for carbonate- and detrital-dominated sites, calculated based on the data
596 from Table 2, marked with red and black dotted lines, respectively.

597 In essence, the retention of a narrow band of colder bottom-water temperatures (-0.3 to
598 2.14 °C) regardless of the host sediment type, as stressed by this study, is a requirement
599 for the dissolution of opal to persist across the water-sediment interface, while pore water
600 remains undersaturated. Wide temperature ranges (-5 to 25 °C) and therefore warmer
601 bottom-water temperatures (commonly > 3 °C, according to Abraham et al., 2013), as
602 followed by Frings (2017), accelerate dissolved silica concentrations quickly towards

https://doi.org/10.5194/os-2019-121
Preprint. Discussion started: 3 January 2020

603 equilibrium solubility values in sediment pore water (after Williams and Crerar, 1985;
604 Van Cappellen et al., 2002), which lead the silica dissolution rate and its recycling to
605 cease. Therefore, unsurprisingly no relationship is observed between the silica exchange
606 rates and the warmer bottom-water temperatures. Excluding the warmer temperatures,
607 flux-temperature diagram of Frings (2017) illustrates a good correlation between these
608 parameters.

609 6.4 Biogenic silica burial efficiency

610 The fractions of biogenic opal recycled and buried in the sediment from the researched
611 sites are clearly a function of the opal rain rate (Table 3 and Fig. 11), but this relationship
612 is not straightforward. At low sedimentation rates, corresponding to lower opal rain rates
613 in this study, a reduced fraction of the opal becomes buried due to its prolonged exposure
614 across the benthic layer. Here, the lower rates of opal rain at the seafloor correspond to a
615 higher silica content become recycled by extensive dissolution of opal. Conversely, at
616 sites with relatively high sedimentation rates for biogenic silica, corresponding to higher
617 opal rain rates, the burial is maximised as the deposited opal particles remain at the
618 water-sediment interface only for a short time. Further, the detrital nature of benthic
619 layers that have higher sedimentation rates among the ODP stations (Sites 1150 and
620 1175) places a constraint on significant removal by dissolution of biosilica from sediment
621 to the water column. High sedimentation rates combined with the detrital composition of
622 host sediment thus causes opal to dissolve slowly near the water-sediment interface as it
623 is removed from the dissolution zone due to comparatively rapid burial (after Rabouille et
624 al., 1997; the burial efficiency of opal in detrital sites reached elevated values up to 53%;

https://doi.org/10.5194/os-2019-121
Preprint. Discussion started: 3 January 2020

625 Fig. 11). Even for sites with low sedimentation rates, a higher mean buried flux of opal in
626 detrital-dominated (~11%) than carbonate benthic layers (~5%) (Table 3) is because the
627 aluminosilicates form a coating on opal particles (Michalopoulos and Aller, 1995), which
628 reduces their solubility and leads to a lower recycled silica flux in detrital sites.

629 Table 3. Site-specific benthic flux, burial flux, and rain rate of biogenic opal calculated
630 using the early diagenetic equations 1.3, 1.4, and 1.5, respectively. Also shown are the
631 relative diffused and buried fluxes (in percentage) at each site. No. = the identification
632 number of the ODP sites presented in Figure 1, J_0 = benthic flux of dissolved silica, BSi_{acc}
633 = opal burial flux, and BSi_{rain} = opal rain rate.

No.	Host lithology	J_0, mol m^{-2} yr^{-1}	BSi_{acc}, kg m^{-2} yr^{-1}	BSi_{rain}, mol m^{-2} yr^{-1}	Recycled flux, %	Buried flux, %
1	Detrital	1.03	0.002	1.06	97.2	2.8
2	Detrital	0.79	0.001	0.81	97.5	2.5
3	Detrital	0.72	0.003	0.77	93.5	6.5
4	Detrital	0.88	0.002	0.91	96.7	3.3
5	Detrital	1.24	0.01	1.39	89.2	10.8
6	Detrital	1.35	0.007	1.46	92.5	7.5
9	Detrital	1.13	0.006	1.22	92.6	7.4
10	Detrital	0.59	0.005	0.67	88.1	11.9
11	Detrital	0.78	0.002	0.81	96.3	3.7
12	Detrital	1.05	0.004	1.11	94.6	5.4
13	Detrital	2.14	0.05	2.97	72	28
14	Detrital	1.67	0.01	1.82	91.8	8.2
15	Detrital	1.97	0.007	2.08	94.7	5.3
16	Detrital	1.03	0.07	2.19	47	53
18	Detrital	0.97	0.003	1.02	95.1	4.9
7	Carbonate	2.02	0.006	2.11	95.7	4.3
8	Carbonate	1.71	0.003	1.76	97.2	2.8
17	Carbonate	1.06	0.002	1.09	97.2	2.8
19	Carbonate	0.81	0.001	0.83	97.6	2.4
20	Carbonate	0.73	0.001	0.75	97.3	2.7
21	Carbonate	1.37	0.02	1.67	82	18
22	Carbonate	2.21	0.008	2.33	94.8	5.2

https://doi.org/10.5194/os-2019-121
Preprint. Discussion started: 3 January 2020

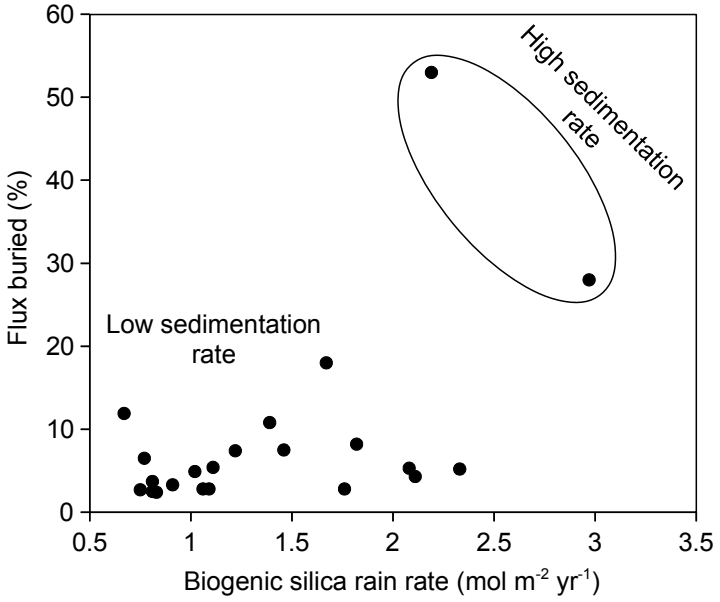

634 Figure 11. The fraction of solid silica buried as a function of the opal rain rate
635 emphasising the role of sedimentation rate in the preservation of biogenic silica.

636 6.5 Controls on the precipitation of low temperature near-surface opal-CT

637 Numerous studies have shown temperature and time are the most efficient controls on
638 transformation of biogenic to diagenetic opal (e.g., Kastner et al., 1977; Kastner and
639 Gieskes, 1983; Kuramoto et al., 1992; Nobes et al., 1992; Hesse and Schacht, 2011).
640 Dissolution rate of opal-A typically controls the overall rate of opal-A to opal-CT
641 transformation under various chemical conditions (Williams et al., 1985; Wrona et al.,
642 2017). This rate-controlling process brings silica in pore waters to values approaching
643 solubility level of disordered opal-CT as the surface area of opal-A decreases with
644 dissolution, and opal-CT enters the accumulation stage (Hinman, 1998).

https://doi.org/10.5194/os-2019-121
Preprint. Discussion started: 3 January 2020

645 Opal-CT precipitates following opal-A dissolution, when sediment temperatures are
646 between 35–50 °C (comparable to burial depths of hundreds of metres) (Behl, 1999),
647 although in some depositional settings this is as low as 17–21 °C (Matheney and Knauth,
648 1993). Nevertheless, there are uncommon occurrences of early diagenetic young (0.4–4
649 Ma) opal-CT porcellanites and cherts at low temperatures commonly between 0 and 4 °C
650 within near-surface sediments. The best known near-seabed recordings of opal-CT
651 growth have been reported from the Antarctic marine sediment (Bohrmann et al., 1990;
652 Botz and Bohrmann, 1991).

653 Until now, there has only been speculation concerning the controls on precipitation of
654 opal-CT in these near-surface sediments. Model predictions of early diagenetic silica
655 precipitation within the topmost layers of studied ODP cores have attempted to clarify
656 whether or not surface temperatures account for accumulation of opal-CT in the topmost
657 sediment. As the Arrhenius plot of early diagenetic transformation of silica (represented
658 by *ln k*) over a narrow temperature range (0–3 °C) is based on 22 ODP surficial sediment
659 sites (Fig. 12) having a global distribution, it is applicable to other ocean basins. Here,
660 this model is used to predict the transformation of silica at the ODP Leg 120 Site 751
661 from the Kerguelen Plateau in Antarctic. Botz and Bohrmann (1991) report occurrence of
662 pure opal-CT porcellanite at the depth of ~14 mbsf for this site. The linear regression for
663 silica diagenesis, with the slope (activation energy) and intercept (pre-exponential factor)
664 being 0.136 and ~-34.03, respectively, estimates a transformation rate constant of 1.7 ×
665 10^{-15} s^{-1} for the sediment at ~14 mbsf (~0.12 °C) for Site 751. Assuming an age of 3 Ma
666 for the porcellanites, opal-A to opal-CT transformation at this site was predicted using the

https://doi.org/10.5194/os-2019-121
Preprint. Discussion started: 3 January 2020

658 first-order translation of rate coefficient into a transformation ratio following:

659 $$1-e^{-kt} = 1-e^{-(1.7\times10^{-15}\times3\times10^{6}\times365\times24\times3600)} = \sim 0.15 \quad (1.6)$$

660 where k is the precipitation rate constant (in s^{-1}) and t is time (in s). The term e^{-kt} in
661 Equation 1.6 is the relative amount of untransformed biogenic silica (according to the
662 first-order rate law: $A/A_0 = e^{-kt}$, where A and A_0 are the remaining and initial amount of
663 biogenic opal (in volume %), respectively).

664 The linear rate law (Fig. 12 and Equation 1.6) slightly overpredicted the ODP-extracted
665 transformation ratio of ~0.1 for Site 751 (Shipboard Scientific Party, 1989) by 0.05. At
666 the water-sediment interface (temperature = -0.3°C), the linear model predicted well the
667 transformation ratio equal to a measured value of 0. The close correspondence between
668 the predicted and measured values (Fig. 13) validates this model for estimating silica
669 transformation rates and ratios in near-surface sediments for different ocean settings.

670 The agreement between the depth variability of model-predicted transformation ratios
671 observed at Site 751 and the temperature increase in the near-surface sediments initiated
672 from the seafloor down-core along the site-specific geothermal gradient to the depth of
673 opal-CT formation suggests that there may be controls from these low temperatures on
674 accumulation of opal-CT porcellanites close to the seabed. Further, the present-day
675 temperatures measured at the depth of opal-CT porcellanite agrees well with the isotopic
676 opal-CT formation temperature range of 0 to 1 °C (Friedman and O'Neil, 1976),

https://doi.org/10.5194/os-2019-121
Preprint. Discussion started: 3 January 2020

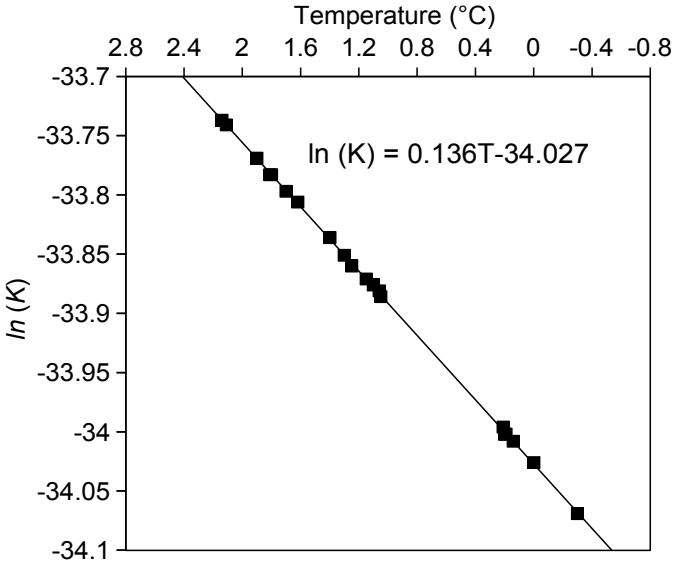

677 Figure 12. Linear transformation rate in the analysed surface sediments. The rate
678 coefficients were adjusted using an activation energy of 85000 J mol^{-1} (Icenhower and
679 Dove, 2000) to represent early diagenetic re-precipitation process within the sediment.

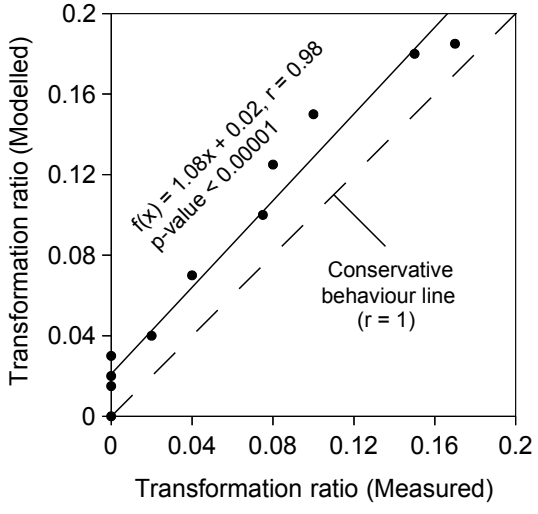

680 Figure 13. Model predicted versus measured transformation ratios of opal-A to opal-CT,
681 Site 751. The measured values were derived from Shipboard Scientific Party (1989).

https://doi.org/10.5194/os-2019-121
Preprint. Discussion started: 3 January 2020

682 suggesting no deviation from the general trend of temperature change parallel to the
683 thermal gradient with the precipitation of opal-CT.

684 The accumulation of diagenetic silica under such low temperature conditions is, however,
685 in contrast with the established models of later diagenetic precipitation of opal-CT within
686 deep-sea sediments, which require the dominance of higher temperatures (commonly
687 between 18 and 56 °C; Pisciotto, 1981) for transformation. Further, the widely accepted
688 inverse correlation between age and formation temperature of opal-CT, implying silica
689 transformation at higher temperatures in young deposits and vice versa (Hein et al., 1978;
690 Giles, 1997; Neagu, 2011), challenges low surface temperatures being a major control on
691 precipitation of opal-CT near the seabed in Site 751. Alternative explanation for unusual
692 deposition of near-surface opal-CT may be drawn from relationship between solubility
693 and surface area of biogenic silica. Considering the surface area of opal-A is ranging
694 between 19 and 350 m^2/g (Hurd, 1973), the steady-state solubility of skeletal silica is
695 likely to quickly approach the equilibrium solubility for this surface area (i.e., 120 ppm,
696 Tobler et al., 2017) as dissolution is rapid relative to nucleation and growth of other silica
697 containing phases (Williams et al., 1985). It is assumed that, in the context of surficial
698 opal-CT deposits at Site 751, age plays a critical role more important than temperature.
699 The solubility and specific surface area decrease with age in biosiliceous sediments
700 (Hurd, 1983). It is therefore possible that an elapsed time of near 4 Ma has aged opal-A
701 to the point that changes in particle size or surface area have produced minor effects on
702 solubility. This process could possibly speed up the silica transformation in Site 751,
703 allowing opal-CT of a specific surface area within the range of the opal-A surface area to

https://doi.org/10.5194/os-2019-121
Preprint. Discussion started: 3 January 2020

694 nucleate from the pore water supersaturated with opal-CT earlier than it otherwise would.

695 **7 Conclusions**

696 Empirical models specified for two deep-sea sediment types hosting biogenic silica—
697 detrital and carbonate—are developed to predict variations in dissolution rates of
698 deposited biogenic silica and benthic fluxes of produced silicic acid with present-day
699 bottom-water temperatures across the benthic layer for 22 representative ODP sites. The
700 significant variables in the models are the opal-A content of the benthic layer, the
701 temperature-dependent kinetic constant, the saturation concentration of dissolved silica,
702 and bottom-water temperature. Variability in the silica exchange rates in relation to
703 surface temperatures is more pronounced when the functional association of temperature
704 on saturation levels and dissolution kinetics is involved in prediction of dissolution rate
705 and benthic flux. A subtler increase in dissolution rates and benthic fluxes with
706 temperature in detrital-hosted sediments, as opposed to the large increases in the silica
707 exchange rates for carbonate sites, is because the detrital matter incorporated into the
708 surface lattice of biosilica markedly limits its solubility and reactivity. This modification
709 of silica early diagenetic reactions in presence of detrital matter has led to a higher opal
710 burial efficiency for clay-dominated stations with different opal rain rates. The mismatch
711 between the model-calculated silica exchange rates determined in this work and previous
712 values from other research is attributed to the temperature differences and large
713 discrepancies in sediment composition between this study and the others.

714 Tough linear expression of early diagenetic transformation of biogenic to diagenetic opal

https://doi.org/10.5194/os-2019-121
Preprint. Discussion started: 3 January 2020

715 declares possible surface temperature controls on accumulation of low temperature (0–4
716 °C) opal-CT in young sediments (< 4 Ma) near the seabed in the Antarctic Site 751, the
717 established inverse temperature-time relation in silica diagenesis requires precipitation of
718 young opal-CT deposits at higher temperatures. Silica solubility and specific surface area
719 relationship provides more reliable explanation in this situation, where a < 4 Ma time has
720 been sufficient to reach opal the point that further surface area decreases have produced
721 negligible effects on solubility, which allows for earlier precipitation of opal-CT.

722 **Acknowledgments**

723 This paper is based on the sixth chapter of the D.Phil. thesis completed by S.V. at the
724 Department of Earth Sciences, University of Oxford. S.V. gratefully acknowledges Joe
725 Cartwright and Nick Tosca for serving as the thesis supervisors. This work used data
726 derived from the Ocean Drilling Program and the International Ocean Discovery Program
727 database. The authors declare no conflicts of interest.

728 **References**

729 Abraham, J. P., Baringer, M., Bindoff, N. L., Boyer, T., Cheng, L. J., Church, J. A.,
730 Conroy, J. L., Domingues, C. M., Fasullo, J. T., Gilson, J., Goni, G., Good, S. A.,
731 Gorman, J. M., Gouretski, V., Ishii, M. 2013. A review of global ocean temperature
732 observations: Implications for ocean heat content estimates and climate change, *Reviews*
733 *of Geophysics*, v. 51, p. 450–483.

734 Arrhenius, S. 1889. Über die Reaktionsgeschwindigkeit bei der Inversion von

https://doi.org/10.5194/os-2019-121
Preprint. Discussion started: 3 January 2020

735 Rohrzucker durch Säuren, *Zeitschrift für Physikalische Chemie*, v. 4, p. 226–248.

736 Atkins, P., and de Paola, J. 2006. Physical Chemistry (8th Edition), Oxford University
737 Press, Oxford, 1149 p.

738 Behl, R. J. 1999. Since Bramlette (1946): The Miocene Monterey Formation of
739 California revisited. *In* Moores, E. M., Sloan, D., and Stout, D. L. (Eds.), Classic
740 Cordilleran Concepts: A View from California, Geological Society of America Special
741 Papers, v. 338, p. 301–313.

742 Berner, R. A. 1980. Early Diagenesis: A Theoretical Approach, Princeton University
743 Press, Princeton, 241 p.

744 Blum, P. 1997. Physical properties handbook: A guide to the shipboard measurement of
745 physical properties of deep-sea cores, Ocean Drilling Program, Texas A&M University,
746 Technical Note 26, 117 p.

747 Boggs, S. 2009. Petrology of Sedimentary rocks (2nd Edition), Cambridge University
748 Press, Cambridge, 600 p.

749 Bohrmann, G., Kuhn, G., Abelmann, A., Gersonde, R., and Fütterer, D. 1990. A Young
750 Porcellanite Occurrence from the Southwest Indian Ridge, *Marine Geology*, v. 92, p.
751 155–163.

752 Botz, R., and Bohrmann, G. 1991. Low-temperature opal-CT precipitation in Antarctic
753 deep-sea sediments: evidence from oxygen isotopes, *Earth and Planetary Science*

https://doi.org/10.5194/os-2019-121
Preprint. Discussion started: 3 January 2020

754 *Letters*, v. 107, p. 612–617.

755 Canfield, D. E., Erik, K., and Bo, T. 2005. The silicon cycle. *In* Canfield, D. E., Erik, K.,
756 and Bo, T (Eds.), Advances in Marine Biology, Academic Press, v. 48, p. 441-463.

757 Davies, R. J., and Cartwright, J. 2002. A fossilized Opal A to Opal C/T transformation on
758 the northeast Atlantic margin: Support for a significantly elevated palaeogeothermal
759 gradient during the Neogene?, *Basin Research*, v. 14, p. 467–486.

760 Dixit, S., and Van Cappellen, P. 2003. Predicting benthic fluxes of silicic acid from deep-
761 sea sediments, *Journal of Geophysical Research: Oceans*, v. 108, No. C10, 3334, doi:
762 10.1029/2002JC001309.

763 Dixit, S., Van Cappellen, P., and van Bennekom, A. J. 2001. Processes controlling
764 solubility of biogenic silica and pore water build-up of silicic acid in marine sediments,
765 *Marine Chemistry*, v. 73, p. 333–352.

766 Dove P. M., and Rimstidt. J. D. 1994. Silica-water interactions. *In* Heaney, P. J., Prewitt,
767 C. T., and Gibbs, G. V. (Eds.), Silica: Physical behavior, geochemistry, and materials
768 applications, Reviews in Mineralogy, Mineralogical Society of America, Washington, v.
769 29, p. 259–308.

770 Dralus, D., Lewan, M. D., and Peters, K. 2015. Kinetics of the Opal-A to Opal-CT Phase
771 Transition in Low- and High-TOC Siliceous Shale Source Rocks, American Association
772 of Petroleum Geologists Annual Convention & Exhibition, Denver, Colorado.

773 Fisher, A. T., and Becker, K. 1993. A guide to ODP tools for downhole measurements,

https://doi.org/10.5194/os-2019-121
Preprint. Discussion started: 3 January 2020

774 Ocean Drilling Program, Texas A&M University, Technical Note 10 (Revised), 131 p.

775 Friedman, I., and O'Neil, J. R. 1976. Compilation of stable isotope fractionation factors
776 of geochemical interest. *In* Fleischer, M. (Ed.), Data of Geochemistry (6th Edition),
777 United States Geological Survey, Professional Paper 440–KK.

778 Frings, P. 2017. Revisiting the dissolution of biogenic Si in marine sediments: a key term
779 in the ocean Si budget, *Acta Geochimica*, v. 36, p. 429–432.

780 Gieskes, J. M., Gamo, T., and Brumsack, H. 1991. Chemical Methods for Interstitial
781 Water Analysis aboard JOIDES Resolution, Ocean Drilling Program, Texas A&M
782 University, Technical Note 15, 60 p.

783 Giles, M. R. 1997. Diagenesis: A Quantitative Perspective, Kluwer Academic Publishers,
784 Dordrecht, The Netherlands, 526 p.

785 Hein, J. R., and Parrish, J. T. 1987. Distribution of siliceous deposits in space and time.
786 *In* Hein, J. R. (Ed.), Siliceous Sedimentary Rock-Hosted Ores and Petroleum, Van
787 Nostrand Reinhold, New York, p. 10–57.

788 Hein, J. R., Scholl, D. W., Barron, J. A., Jones, M. G., and Miller, J. 1978. Diagenesis of
789 late Cenozoic diatomaceous deposits and formation of the bottom simulating reflector in
790 the southern Bering Sea, *Sedimentology*, v. 25, p. 155–181.

791 Hesse, R., and Schacht, U. 2011. Early diagenesis of deep-sea sediments. *In* Hüneke, H.,
792 Mudler, T., et al. (Eds.), Deep-sea sediments, Developments in Sedimentology, v. 63,
793 Elsevier, Amsterdam, p. 557–713.

https://doi.org/10.5194/os-2019-121
Preprint. Discussion started: 3 January 2020

794 Hinman, N. W. 1998. Sequences of silica phase transitions: effects of Na, Mg, K, Al, and
795 Fe ions, *Marine Geology*, v. 147, p. 13–24.

796 Hurd, D. C. 1973. Interactions of biogenic opal, sediment and seawater in the Central
797 Equatorial Pacific, *Geochimica et Cosmochimica Acta*, v. 37, p. 2257–2282.

798 Hurd, D. C. 1983. Physical and chemical properties of siliceous skeletons. *In* Aston, S. R.
799 (Ed.), Silicon Geochemistry and Biogeochemistry, Academic Press, London, p. 187–244.

800 Icenhower, J. P., and, Dove, P. M. 2000. The dissolution kinetics of amorphous silica into
801 sodium chloride solutions: effects of temperature and ionic strength, *Geochimica et*
802 *Cosmochimica Acta*, v. 64, p. 4193–4203.

803 Ingle, J. C., Jr. 1980. Cenozoic paleobathymetry and depositional history of selected
804 sequences within the southern California continental borderland, *Cushman Foundation*
805 *for foraminiferal Research Special Publication*, no. 19, p. 163–195.

806 Ingle, J. C., Jr. 1981. Origin of Neogene diatomites around the north Pacific rim. *In*
807 Garrison, R. E., and Douglas, R. G. (Eds.), The Monterey Formation and related siliceous
808 rocks of California, Society of Economic Paleontologists and Mineralogists Publication,
809 Pacific Section, v. 15, p. 159–180.

810 International Ocean Discovery Program. 2018. http://iodp.tamu.edu/database/

811 Joint, I., and A. Pomroy. 1993. Phytoplankton biomass and production in the southern
812 North Sea, *Marine Ecology Progress Series*, v. 99, p. 169–182.

https://doi.org/10.5194/os-2019-121
Preprint. Discussion started: 3 January 2020

813 Kastner, M, and Gieskes, J. M. 1983. Opal-A to opal-CT transformation: A kinetic study.
814 *In* Iijima, A., Hein, J. R., and Siever, R. (Eds.), Siliceous Deposits in the Pacific Region,
815 Amsterdam, Elsevier Science Publishing Company, p. 211–227.

816 Kastner, M., Keene, J. B., and Gieskes, J. M. 1977. Diagenesis of siliceous oozes – I.
817 Chemical controls on the rate of opal-A to opal-CT transformation – an experimental
818 study, *Geochimica et Cosmochimica Acta*, v. 41, p. 1041–1059.

819 Kidder, D. L., and Erwin, D. H. 2001. Secular distribution of biogenic silica through the
820 Phanerozoic: comparison of silica-replaced fossils and bedded cherts at the series level,
821 *The Journal of Geology*, v. 109, p. 509–522.

822 Kuramoto, S., Tamaki, K., Langseth, M. G., Nobes, D. C., Toluyama, H., Pisciotto, K.
823 A., and Taira, A. 1992. Can opal-A/opal-CT BSR be an indicator of the thermal structure
824 of the Yamato Basin, Japan Sea?. *In* Tamaki, K., Suyehiro, K., Allan, J., McWilliams,
825 M., et al. (Eds.), Proceedings of the Ocean Drilling Program, Scientific Results, College
826 Station, Texas , v. 127/128, p. 1145–1156.

827 Lancelot, Y. 1973. Chert and silica diagenesis in sediments from the central Pacific. *In*
828 Winterer P. L., Ewing, J. I., et al. (Eds.), Initial Reports of the Deep Sea Drilling Project,
829 U.S. Government Printing Office, Washington, v. 17, p. 377–405.

830 Libes, S. M. 1992. An Introduction to Marine Biogeochemistry, John Wiley and Sons,
831 New York, 734 p.

832 Marsaglia, K., Milliken, K., and Doran, L. 2013. Smear slides of marine mud for IODP

https://doi.org/10.5194/os-2019-121
Preprint. Discussion started: 3 January 2020

833 core description, Volume I. Part 1: Methodology and atlas of siliciclastic and
834 volcanogenic components. Integrated Ocean Drilling Program, Technical Note 1, 236 p.

835 Martin, W. R., and Sayles, F. L. 2003. The Recycling of Biogenic Material at the
836 Seafloor. *In* Holland, H, D., and Turekian, K, K. (Eds.), Sediments, Diagenesis, and
837 Sedimentary Rocks: Treatise on Geochemistry (2nd Edition), Elsevier Science, v. 7, p. 37–
838 65.

839 Matheney, R. K., and Knauth, L. P. 1993. New isotopic temperature estimates for early
840 silica diagenesis in bedded cherts, *Geology*, v. 21, p. 519–522.

841 Mazzullo, J. M., and Graham, A. G. 1988. Handbook for shipboard sedimentologists,
842 Ocean Drilling Program, Texas A&M University, Technical Note 8, 70 p.

843 Meile, C., and Van Cappellen, P. 2003. Global estimates of enhanced solute transport in
844 marine sediments, *Limnology and Oceanography*, v. 48, p. 777–786.

845 Michalopoulos, P., and Aller, R. C. 1995. Rapid Clay Mineral Formation in Amazon
846 Delta Sediments, *Science*, v. 270, p. 614–617.

847 Muttoni, G., and Kent, D. V. 2007. Widespread formation of cherts during the early
848 Eocene climate optimum, *Palaeogeography, Palaeoclimatology, Palaeoecology*, v. 253,
849 p. 348–362.

850 Neagu, R. C. 2011. The relationship between biogenic silica diagenesis and the physical
851 properties of sediments studied using seismic and well data, PhD thesis, Cardiff

https://doi.org/10.5194/os-2019-121
Preprint. Discussion started: 3 January 2020

852 University, 275 p.

853 Neagu, R. C., Cartwright, J., Davies, R. J., and Jensen, L. 2010. Fossilisation of a silica
854 diagenesis reaction front on the mid-Norwegian margin, *Marine and Petroleum Geology*,
855 v. 27, p. 2141–2155.

856 Nobes, D. C., Murray, R. W., Kuramoto, S., Pisciotto, K. A., and Holler, P. 1992. Impact
857 of silica diagenesis on physical property variations. *In* Pisciotto, K. A., Ingle, J. C., Jr.,
858 von Breymann, M. T., Barron, J., et al. (Eds.), Proceedings of the Ocean Drilling
859 Program, Scientific Results, College Station, Texas, v. 127/128 (Pt. 1), p. 3–31.

860 Noymer, A. 2008. Alpha, Significance Level of Test. *In* P. J., Lavrakas (Ed.),
861 Encyclopedia of Survey Research Methods, Sage Publications, Thousand Oaks,
862 California.

863 Ocean Drilling Program Site Maps. 2009. [Drawing]. In Ocean Drilling Program,
864 Accessed 30 August 2019, http://www-odp.tamu.edu/sitemap/sitemap.html
865 Oehler, T. 2014. Seasonal variations of benthic carbon and nutrient fluxes in the southern
866 North Sea, PhD thesis, University of Bremen, 116 p.

867 Park, J., Norman, D., McLin, K., and Moore, J. 2006. Modelling amorphous silica
868 precipitation: a strategy to reduce silica precipitation near Coso injection wells,
869 Proceedings, Thirty-First Workshop on Geothermal Reservoir Engineering, Stanford
870 University, California, January 30-February 1, p. 267–274.

871 Pisciotto, K. A. 1981. Diagenetic trends in the siliceous facies of the Monterey Shale in

https://doi.org/10.5194/os-2019-121
Preprint. Discussion started: 3 January 2020

872 the Santa Maria region, California, *Sedimentology*, v. 28, p. 547–571.

873 Rabinowitz, P. D., and Garrison, L. E. 1985. Operational and Laboratory Capabilities of
874 "JOIDES Resolution", Ocean Drilling Program, Texas A&M University, Technical Note
875 2, 34 p.

876 Rabouille, C., Gaillard, J.-F., Tréguer, P., and Vincendeau, M.-A. 1997. Biogenic silica
877 cycling in surfacial sediments across the Polar Front of the Southern Ocean (Indian
878 Sector), *Deep Sea Research Part II: Topical Studies in Oceanography*, v. 44, p. 1151–
879 1176.

880 Ragueneau, O., Regaudie-de-Gioux, A., Moriceau, B., Gallinari, M., Vangriesheim, A.,
881 Baurand, F., and Khripounoff. A. 2009. A benthic Si mass balance on the Congo margin:
882 Origin of the 4000m Dsi anomaly and implications for the transfer of Si from land to
883 ocean, *Deep Sea Research Part II: Topical Studies in Oceanography*, v 56, p. 2197–
884 2207.

885 Ragueneau, O., Tréguer, P., Leynaert, A., Anderson, R. F., Brzezinski, M. A., DeMaster,
886 D. J., Dugdale, R. C., Dymond, J., Fischer, G., François, R., Heinze, C., Maier-Reimer,
887 E., Martin-Jézéquel, V., Nelson, D. M., and Quéquiner, B. 2000. A review of the Si cycle
888 in the modern ocean: recent progress and missing gaps in the application of biogenic opal
889 as a paleoproductivity proxy, *Global and Planetary Change*, v. 26, p. 317–365.

890 Rashid, M. A. 1985. Geochemistry of Marine Humic Compounds, Springer-Verlag, New
891 York, 300 p.

https://doi.org/10.5194/os-2019-121
Preprint. Discussion started: 3 January 2020

892 Rickert, D. 2000. Dissolution kinetics of biogenic silica in marine environments (Reports
893 on Polar Research 351), PhD thesis, Alfred Wegener Institute for Polar and Marine
894 Research, 211 p.

895 Sarmiento, J. L., Simeon, J., Gnanadesikan, A., Gruber, N., Key, R. M., and Schlitzer, R.
896 2007. Deep ocean biogeochemistry of silicic acid and nitrate, *Global Biogeochemical*
897 *Cycles*, v. 21, GB1S90, doi:10.1029/2006GB002720.

898 Schink, D. R., Guinasso, N. L., Jr., and Fanning, K. A. 1975. Processes affecting the
899 concentration of silica at the sediment-water interface of the Atlantic Ocean, *Journal of*
900 *Geophysical Research*, v. 80, p. 3013–3031.

901 Shipboard Scientific Party. 1989. Site 751. *In* Schlich, R., Wise, S. W., Jr., et al. (Eds.),
902 Proceedings of the Ocean Drilling Program, Initial Reports, College Station, Texas, v.
903 120, p. 339–373.

904 Shipboard Scientific Party. 1990a. Site 794. *In* Tamaki, K., Pisciotto, K., Allan, J., et al.
905 (Eds.), Proceedings of the Ocean Drilling Program, Initial Reports, College Station,
906 Texas, v. 127, p. 71–167.

907 Shipboard Scientific Party. 1990b. Site 798. *In* Ingle, J. C., Jr., Suyehiro, K., von
908 Breymann, M. T., et al. (Eds.), Proceedings of the Ocean Drilling Program, Initial
909 Reports, College Station, Texas, v. 128, p. 121–236.

910 Siever, R. 1992. The silica cycle in the Precambrian, *Geochimica et Cosmochimica Acta*,
911 v. 56, p. 3265–3272.

https://doi.org/10.5194/os-2019-121
Preprint. Discussion started: 3 January 2020

912 Terry, R. D., and Chilingarian, G. V. 1955. Summary of "Concerning some additional
913 aids in studying sedimentary formations" by M. S. Shvetsov, *Journal of Sedimentary*
914 *Petrology*, v. 25, p. 229–234.

915 Tobler, D. J., Stawski, T. M., and Benning, L. G. 2017. Silica and Alumina Nanophases:
916 Natural Processes and Industrial Applications. *In* Van Driessche, A., Kellermeier, M.,
917 Benning, L., and Gebauer, D. (Eds.), New Perspectives on Mineral Nucleation and
918 Growth. Springer, Cham, p. 293–316.

919 Tréguer, P. J., and De La Rocha, C. L. 2013. The world ocean silica cycle, *Annual*
920 *Review of Marine Science*, v. 5, p. 477–501.

921 Tréguer, P. J., Nelson, D. M., van Bennekom, A. J., DeMaster, D. J., Leynaert, A., and
922 Quéguiner, B. 1995. The silica balance in the world ocean: A reestimate, *Science*, v. 268,
923 p. 375–379.

924 Ullman, W. J., and Aller, R. C. 1982. Diffusion coefficients in near-shore sediments,
925 *Limnology and Oceanography*, v. 27, p. 552–556.

926 Van Cappellen, P., and Qiu, L. 1997a. Biogenic silica dissolution in sediments of the
927 Southern Ocean: I. Solubility, *Deep Sea Research Part II: Topical Studies in*
928 *Oceanography*, v. 44, p. 1109–1128.

929 Van Cappellen, P., and Qiu, L. 1997b. Biogenic silica dissolution in sediments of the
930 Southern Ocean: II. Kinetics, *Deep Sea Research Part II: Topical Studies in*
931 *Oceanography*, v. 44, p. 1129–1149.

https://doi.org/10.5194/os-2019-121
Preprint. Discussion started: 3 January 2020

932 Van Cappellen, P., Dixit, S., and Van Beusekom, J. 2002. Biogenic silica dissolution in
933 the oceans: Reconciling experimental and field-based dissolution rates, *Global*
934 *Biogeochemical Cycles*, v. 16, 1075, doi:10.1029/2001GB001431.
935 Van der Weijden, A. J., and Van der Weijden, C. H. 2002. Silica fluxes and opal
936 dissolution rates in the northern Arabian Sea, *Deep Sea Research Part I: Oceanographic*
937 *Research Papers*, v. 49, p. 157–173.

938 Varkouhi, S. 2018. Biogenic silica diagenesis under early burial in hemipelagic marine
939 sediments, D.Phil. thesis, University of Oxford, 428 p.

940 Wildish. D. J. 2001. Benthic Boundary Layer Effects. *In* Steele, J. H., Thorpe, S. A., and
941 Turekian, K. K. (Eds.), Encyclopedia of Ocean Sciences: Marine Biology, Academic
942 Press, San Diego, p. 199–208.

943 Williams, L. A., and Crerar, D. A. 1985. Silica diagenesis, II. General mechanisms,
944 *Journal of Sedimentary Petrology*, v. 55, p. 312–321.

945 Williams, L. A., Parks, G. A., and Crerar, D. A. 1985. Silica diagenesis, I. Solubility
946 controls, *Journal of Sedimentary Petrology*, v. 55, p. 301–311.

947 Wrona, T., Jackson, C. A.-L., Huuse, M., and Taylor, K. G. 2017. Silica diagenesis in
948 Cenozoic mudstones of the North Viking Graben: physical properties and basin
949 modelling, *Basin Research*, v. 29, p. 556–575.

950 Yamano, M., Hamamoto, H., Kawada, Y., and Goto, S. 2014. Heat flow anomaly on the
951 seaward side of the Japan Trench associated with deformation of the incoming Pacific

https://doi.org/10.5194/os-2019-121
Preprint. Discussion started: 3 January 2020

952 plate, *Earth and Planetary Science Letters*, v. 407, p. 196–204.